Copy 229
RM L52L23

NACA RM L52L23

7398

NACA

RESEARCH MEMORANDUM

A TRANSONIC WIND-TUNNEL INVESTIGATION OF THE

EFFECTS OF BODY INDENTATION, AS SPECIFIED BY THE

TRANSONIC DRAG-RISE RULE, ON THE AERODYNAMIC

CHARACTERISTICS AND FLOW PHENOMENA OF AN

UNSWEPT-WING—BODY COMBINATION

By Claude V. Williams

Langley Aeronautical Laboratory
Langley Field, Va.

NATIONAL ADVISORY COMMITTEE
FOR AERONAUTICS

WASHINGTON
January 28, 1953

319.98/13

NACA RM L52L23 ~~CONFIDENTIAL~~

NATIONAL ADVISORY COMMITTEE FOR AERONAUTICS

RESEARCH MEMORANDUM

A TRANSONIC WIND-TUNNEL INVESTIGATION OF THE

EFFECTS OF BODY INDENTATION, AS SPECIFIED BY THE

TRANSONIC DRAG-RISE RULE, ON THE AERODYNAMIC

CHARACTERISTICS AND FLOW PHENOMENA OF AN

UNSWEPT-WING—BODY COMBINATION

By Claude V. Williams

SUMMARY

Comparisons of the aerodynamic characteristics and flow phenomena at transonic speeds for two unswept zero-taper-ratio wing-body combinations have been made. The first of these wing-body configurations had a cylindrical afterbody, whereas the afterbody of the second was indented (as specified by the transonic drag-rise rule presented in NACA RM L52H08) in the region of the wing-body juncture so that the axial distribution of the cross-sectional areas normal to the axis of symmetry was the same as that for the cylindrical body alone.

Indentation produced significant relative decreases in the transonic drag-rise increments at moderate lift coefficients as well as at zero-lift conditions. These decreases in the drag-rise increments resulted from appreciable reductions in the strength of the shock-wave system associated with the wing as shown by the tunnel-wall Mach number distributions and the accompanying schlieren flow surveys. Indentation had little effect on the lift and pitching-moment characteristics of the wing-body combinations investigated.

INTRODUCTION

The experimental verification of a new concept (called the transonic drag-rise rule) of the factors governing the zero-lift transonic drag rise of wing-body configurations has been provided by the results of a recent investigation in the Langley 8-foot transonic tunnel (ref. 1). This concept indicates that for thin, low-aspect-ratio wing-body configurations the zero-lift drag rise near the speed of sound is primarily

dependent on the axial distribution of the cross-sectional areas of the combination normal to the axis of symmetry. The validity of this concept is further substantiated by a consideration of the simplifying assumptions that may be made for computing wave drag at low supersonic Mach numbers using linear theory as discussed in reference 2.

The tests of reference 1 also included preliminary evaluations of the zero-lift drag-rise characteristics of special unswept, swept, and delta wing-body combinations designed on the basis of the drag-rise concept. The bodies of these configurations were indented in the region of the wing-body juncture in such a manner that the cross-sectional area of the body of revolution was reduced by an amount equal to the exposed frontal area of the wing at the same axial station. Indenting the bodies in this manner produced wing-body configurations which had axial cross-sectional area distributions equivalent to the area distribution of the cylindrical body alone. The drag-rise characteristics of these indented combinations were compared with the results obtained from tests of these wings with a body that was cylindrical in the region of the wing-body juncture. The comparison indicated that appreciable reductions of the transonic zero-lift drag-rise increments associated with the wing resulted from body indentation. On the basis of these preliminary results, further examinations of the characteristics of the wing-body configurations were made.

This report presents the results of the extended investigations of the unswept wing-body combinations. The objectives of these tests were to evaluate the aerodynamic characteristics of the configurations at moderate angles of attack, to ascertain the flow phenomena responsible for the reduction in the zero-lift drag rise, and, finally, to provide information that might lead to further reductions of the drag rise by additional modifications of the body shape. The tests reported herein were made at Mach numbers of 0.80 through 1.10 and at angles of attack of 0° to 6°. Reynolds number for the investigation varied from 2.4×10^6 to 2.7×10^6 when based on the wing mean aerodynamic chord of 8 inches.

APPARATUS

Tunnel

The investigation was conducted in the Langley 8-foot transonic tunnel. This facility has a dodecagonal slotted test section in which the Mach number is continuously variable through the speed range up to a Mach number of approximately 1.13. Detailed discussions of the design and calibration of this unit are reported in references 3 and 4.

Models

Plan views and dimensional details of the two sting-mounted wing-body combinations investigated are presented in figure 1. Although not shown in figure 1, this investigation also included tests of the cylindrical body without the wing.

The wing of the combinations was the same as that used in the investigation reported in reference 5. This wing is unswept and has an aspect ratio of 4, taper ratio of 0, and symmetrical circular-arc airfoil sections parallel to the vertical plane of symmetry. The wing maximum thickness, located at the 40-percent chord, is 4 percent. The wing was constructed from a solid sheet of aluminum alloy.

The first of the two wing-body configurations investigated, to be identified hereafter in the text as the cylindrical combination, had an afterbody that was cylindrical. The second wing-body configuration, to be referred to as the indented combination, differed from the first in that the body in the region of the wing-body juncture was indented so as to reduce the cross-sectional area of the body of revolution by an amount equal to the exposed frontal area of the wing at the same longitudinal station. Forebody dimensional coordinates are presented in table I. Dimensional coordinates of the indented afterbody are presented in table II. Front and rear three-quarter views of the indented wing-body combination installed on the sting-support system in the test section of the Langley 8-foot transonic tunnel are presented in figure 2. The longitudinal distribution of the total cross-sectional areas normal to the body axis of symmetry for the configurations investigated are presented in figure 3.

The sting model support had approximately the same diameter as the aft end of the model so as to reduce the effects of the model base on the results.

TESTS AND MEASUREMENTS

Tests

The tests reported herein were made at Mach numbers of 0.80 to 1.10 and at angles of attack of 0° to 6°. Reynolds number for the investigation varied from 2.4×10^6 to 2.7×10^6 when based on the wing mean aerodynamic chord of 8 inches.

Force Measurements

The normal, axial, and pitching-moment characteristics of the models were measured by an internally mounted electrical strain-gage force balance. For the Mach number range of this investigation, the repeatability of the lift coefficients presented is judged to be within ±0.004 and for the pitching-moment coefficients, to be within ±0.003. Since several check points were available, the zero-lift drag-coefficient repeatability is estimated to be within ±0.0005. At the lift conditions reported herein, the drag-coefficient repeatability is believed to be within ±0.001.

Model angle of attack was measured by a device new to the 8-foot transonic tunnel. This unit is a fluid-damped, fixed-pendulum, bonded electrical strain-gage unit which was internally mounted within the nose of the model. Variations in the temperature of this angle-of-attack measuring unit caused changes in the zero setting of the instrument; therefore, it was necessary while testing to reference the zero setting of the pendulum unit to that of a Selsyn angle measuring device whose operation is independent of temperature. Considerations of the factors affecting the accuracy of the system indicate the possibility of errors on the order of ±0.1° in model angle of attack.

Static pressures near the base of the model were measured by orifices located in the sting fairing within the model and approximately 1/4 inch ahead of the plane of the model base. All drag coefficients presented herein have been adjusted to the assumption of free-stream static pressure acting on the plane of the model base.

Because of the nature of the flow in the slotted test section, choking and blockage effects both for the zero-lift and low-lift cases presented are negligible, and, therefore, no corrections have been applied for these conditions. As discussed in reference 4, the effects of wall-reflected disturbances on the drag results have been alleviated at all Mach numbers except those near a value of 1.05 by offsetting the model from the tunnel center line and by adjusting the data for base pressures. No data points have been presented for a Mach number of 1.05, and no corrections for these boundary-reflected interference effects have been applied to the data.

Flow-Field Surveys

Rows of static-pressure orifices located along the center line of the test-section panels, which were immediately adjacent to the top and bottom test section panels, were utilized to measure the static pressures necessary for computing the wall Mach number distributions. (See sketch of tunnel configuration for plan-view schlieren surveys in fig. 12(a).)

The maximum random error in indicated Mach number is believed to be on the order of 0.003. Total Mach number deviations generally increased with Mach number but did not exceed 0.006 at stream Mach numbers up to 1.13 (ref. 4).

Schlieren photographs were obtained using the horizontally located, single-pass system described in reference 4. Throughout the tests, the schlieren system remained fixed relative to the tunnel and photographs of the flow field in the two longitudinal locations presented were obtained by movement of the model. For the side-view pictures, the model was offset approximately 10 inches below the tunnel center line with the wings horizontal (see fig. 12(a)). Plan-view photographs were obtained by lowering the model approximately 15 inches below the tunnel center line and axially rotating the model 90° so that the wings were in the vertical plane (see fig. 12(a)).

PRESENTATION OF RESULTS

Force Characteristics

The basic aerodynamic coefficients for the body alone and for the wing-body combinations for various stream Mach numbers M are presented in figures 4 and 5, respectively. Lift coefficient C_L, drag coefficient C_D, and pitching-moment coefficient C_m, are based on the total wing area of 1 square foot (includes area blanketed by body). Drag coefficients have been modified to the assumption of free-stream static pressure acting on the plane of the model base. Pitching-moment coefficients are referred to the quarter chord of the wing mean aerodynamic chord and based on the mean aerodynamic chord of 8 inches.

In figure 6, drag characteristics at zero-lift conditions are presented. The incremental drag coefficient, presented in figure 6, is defined as the drag coefficient at Mach number minus the value of the arithmetical average of the drag coefficients at Mach numbers of 0.80 and 0.85. Presentation of the data in this manner minimizes the effects of skin friction in the analysis. A comparison of the drag characteristics of the wing-body combinations investigated at lift coefficients of 0.2 and 0.4 is presented in figure 7.

A comparison of the maximum lift-drag-ratio characteristics of the complete cylindrical and indented wing-body combinations along with the variation with Mach number of the lift coefficients for maximum lift-drag ratio for the wing-body configurations investigated is presented in figure 8. The wing-plus-interference information presented in figure 9 was obtained by subtracting the body-alone data from that for the wing-body combination.

Average lift-curve slopes, presented in figure 10, were obtained
from those lower portions of the curves of angle of attack against lift
coefficient where approximate linearity existed. In general, departures
from linearity occurred between 4° and 6° angle of attack. The variation
with Mach number of the location of the center of pressure, expressed in
terms of percent of the mean aerodynamic chord, for lift coefficients of
0.2 and 0.4 is presented in figure 11.

Flow Surveys

Schlieren flow surveys and accompanying wall Mach number M_W dis-
tributions at angles of attack of 0° and 3.9° are presented in figures 12
and 13, respectively. In these figures, the drawings of the models are
to the same dimensional scale as the schlieren photographs. With refer-
ence to figure 12(a), the side-view photographs at the top of the page
were taken from the side of the model as indicated in the sketch showing
the tunnel configuration for the side-view surveys. Plan-view photographs,
presented in the center of the figure, were taken with the configuration
shown in the sketch for the plan-view schlieren surveys. The wall Mach
number distributions presented were measured with the model in the position
for the plan-view schlieren surveys as shown in the sketch on figure 12(a).
Throughout figure 12 the distance from the center line of the drawing of
the model to the stream Mach number M represents the scale distance
from the center line of the model to the survey orifices in the tunnel-
wall panels (see fig. 12(a) with reference to dimensions A and B as shown
in the sketch of the tunnel configuration for plan-view schlieren surveys).
As an aid to study of figure 12, the data presented on facing figures are
for the same Mach number and angle of attack and differ only in model
configuration.

Throughout figures 12 and 13, the maximum deviation in Mach number
for any individual schlieren picture from the nominal stream Mach num-
ber was on the order of ±0.01. At the zero-angle-of-attack condition,
the maximum deviation from the nominal angle for the side-view pictures
was approximately +0.05° and -0.15°. In general, because of lost motion
in the angle-of-attack changing mechanism, when the support system and
model were in the position for the plan-view surveys, it was difficult
to set the angle of attack at the desired value. Therefore, the devia-
tions from the desired value of 0° for the plan-view pictures were on
the order of +0.4° and -0.8°, although the deviations were generally
considerably less than these maximum values. At an angle of attack
of 3.9°, the maximum variations from the nominal angle were on the order
of +0.2° and -0.4°.

DISCUSSION

Force Characteristics

Drag at constant lift coefficients.- A comparison of the drag characteristics at zero-lift conditions, as presented in reference 1, is repeated in figure 6 for convenience. At subsonic Mach numbers, body indentation had little effect on the drag characteristics, but at Mach numbers from 0.90 to the highest test value, substantial reductions in the drag rise resulted from body indentation. The maximum reduction was at a Mach number of 1.00 where the value of the incremental drag coefficient for the indented combination was 0.005 or approximately 60 percent less than that for the cylindrical combination. The drag results presented in figure 7 indicate that, near the speed of sound, body indentation reduced the severity of the drag rise at lift coefficients of 0.2 and 0.4 by approximately the same quantitative amount as at zero-lift conditions.

At a lift coefficient of 0.4, the drag coefficients at subcritical Mach numbers for the indented configuration are increased relative to those of the cylindrical combination; however, at Mach numbers near the peak of the drag curves (M = 1.08), the reduction in the drag coefficients was larger than at zero-lift conditions and, therefore, it is possible that, in this Mach number range, indentation had a favorable effect on the drag due to lift.

Maximum lift-drag ratios.- As seen in figure 8, at subsonic speeds, body indentation somewhat reduced the value of the maximum lift-drag ratio relative to that of the cylindrical configuration. However, at Mach numbers of 0.92 and above, increases in the ratio were evident. At a Mach number of 1.00, this increase was on the order of 12 percent. The results of figure 9 indicate that indenting the body also materially increased the wing-plus-interference maximum lift-drag ratio from a Mach number of approximately 0.95 to the highest Mach number of these tests. This increase was greatest near a Mach number of 1.00 and was on the order of 20 percent.

Lift and pitching-moment characteristics.- Reference to figures 5(a), 5(c), 10, and 11 indicates that body indentation had little effect on the lift and pitching-moment characteristics of the configuration.

Flow Phenomena

Angle of attack of 0°.- As indicated in reference 1, because of the particular nature of the flow phenomena near a Mach number of 1.0, the shock field about any configuration extends relatively large distances

away from the configuration. As a result, the major portion of the drag
of the configuration at zero- and low-lift conditions is primarily caused
by the strength of the shock-wave system at a distance from the config-
uration. In view of these facts, the wall Mach number distributions of
this investigation serve as an approximate measure of the strength of the
shock-wave system and, hence, of the drag of the configurations investi-
gated. The distributions of figure 12 show that, for all the Mach numbers
presented, indentation reduced the induced velocities associated with the
wing; hence, it is believed that the relative strength of the shock-wave
system about the indented combination was less than the strength of that
about the cylindrical configuration, and this relative reduction in the
strength of the shock system caused the reduction of the drag coefficients
for the indented wing-body configuration shown by the force measurements
of this investigation.

The schlieren pictures of the flow about the cylindrical wing-body
combination, presented in figures 12(a), 12(c), 12(e), 12(g), and 12(i)
indicate the presence of a shock emanating near the trailing edge of the
wing-body juncture at all test Mach numbers, and at Mach numbers greater
than 1.00, a bow wave ahead of the wing leading edge. At a Mach number
of 1.00, the wing bow wave is ahead of the field of view of the schlieren
pictures as indicated by the tunnel-wall Mach number distributions.

The shock system about the indented wing-body configuration as shown
by the schlieren photographs of figures 12(b), 12(d), 12(f), 12(h), and
12(j) is similar to that about the cylindrical combination to the extent
that the wing-body-juncture trailing-edge shocks and wing bow waves are
present. In addition to the juncture trailing-edge shock and wing bow
wave, there exists about the indented configuration a third shock which
appears to originate near the point of curvature inflection of the forward
portion of the indentation. This shock, identified as shock (a) in
figure 12(f), moves outward and rearward across the wing. The angle of
this shock changes as it crosses the local flow-field discontinuities
associated with the trailing edges of the wing panels (identified as
shock (b) in figure 12(f)). This shock is probably associated with the
rather abrupt contours of the forward portions of the indented region.

Angle of attack of 3.9°.- Figures 13(a) to (c) present a comparison
of the flow about the cylindrical and indented combinations at an angle
of attack of 3.9°. Schlieren pictures for the cylindrical combination
are at the top of the figures, whereas those for the indented combination
are presented in the lower protions of the figures. These figures indicate
that body indentation resulted in a complex flow about the configuration.
The force results of this investigation indicate that the losses through
this shock system were less than those through the shock system about the
cylindrical configuration.

Interpretation of Results

In the absence of detailed pressure-distribution measurements in the region of the indentation, the following discussion must be in the nature of conjecture. The relatively sharp contour of the forward regions of the indentation probably caused a local thickening or separation of the boundary layer in the indentation which was directly responsible for a small increment in drag, but its effect extended beyond this consideration. This local thickening of the boundary layer effectively reduced the depth of the indentation so that the induced velocities in the wing regions were higher than those that would be present had the indentation operated ideally; therefore, because of the higher velocities, the losses through the shock-wave system about the wing were larger and, hence, the drag values for the indented configurations were higher than might be expected had the indentation performed as predicted from considerations of the geometrical area distribution only.

It is believed that modifications of the forward regions of the indentation to eliminate the thickened or separated flow region would reduce the drag-rise increments for this configuration beyond those shown in the present paper.

CONCLUSIONS

The results of an investigation of the effects of an indentation, as specified by the transonic drag-rise rule, of an unswept-wing—body combination lead to the following conclusions:

1. Indentation reduced the transonic drag-rise increments at moderate lift coefficients as well as at zero-lift conditions.

2. The reductions of the drag coefficients resulted in significant increases in the maximum lift-drag ratio at transonic speeds.

3. Body indentation had little effect on the lift and pitching-moment characteristics of the combinations investigated.

4. Reductions in the drag coefficients were accomplished by reducing the strength of the shock-wave system about the configuration.

Langley Aeronautical Laboratory,
    National Advisory Committee for Aeronautics,
        Langley Field, Va.,

10   NACA RM L52L23

REFERENCES

1. Whitcomb, Richard T.: A Study of the Zero-Lift Drag-Rise Characteristics
   of Wing-Body Combinations Near the Speed of Sound. NACA RM L52H08,
   1952.

2. Hayes, Wallace D.: Linearized Supersonic Flow. Rep. No. AL-222, North
   American Aviation, Inc., June 18, 1947.

3. Wright, Ray H., and Ritchie, Virgil S.: Characteristics of a Transonic
   Test Section With Various Slot Shapes in the Langley 8-Foot High-Speed
   Tunnel. NACA RM L51H10, 1951.

4. Ritchie, Virgil S., and Pearson, Albin O.: Calibration of the Slotted
   Test Section of the Langley 8-Foot Transonic Tunnel and Preliminary
   Experimental Investigation of Boundary-Reflected Disturbances.
   NACA RM L51K14, 1952.

5. Estabrooks, Bruce B.: Transonic Wind-Tunnel Investigation of an Unswept-
   Wing-Body Combination at Angles of Attack Up to 24°. NACA RM L52L19,
   1953.

TABLE I.- ORDINATES OF FOREBODY

$\left[\text{All dimensions are in inches.}\right]$

Longitudinal distance measured from body nose	Body radius measured from body center line
0	0
.225	.104
.338	.134
.563	.193
1.125	.325
2.250	.542
3.375	.726
4.500	.887
6.750	1.167
9.000	1.391
11.250	1.559
13.500	1.683
15.750	1.770
18.000	1.828
20.250	1.864
22.500	1.875

TABLE II.- ORDINATES OF INDENTED AFTERBODY

[All dimensions are in inches.]

Longitudinal distance measured from body nose	Body radius measured from body center line
22.500	1.875
23.500	1.875
24.000	1.875
24.500	1.857
25.000	1.807
25.500	1.720
26.000	1.622
26.500	1.521
27.000	1.476
27.500	1.470
28.000	1.487
28.500	1.533
29.000	1.580
29.500	1.642
30.000	1.664
30.500	1.710
31.000	1.743
31.500	1.773
32.000	1.812
32.500	1.837
33.000	1.856
33.500	1.868
34.000	1.875
43.000	1.875

NACA
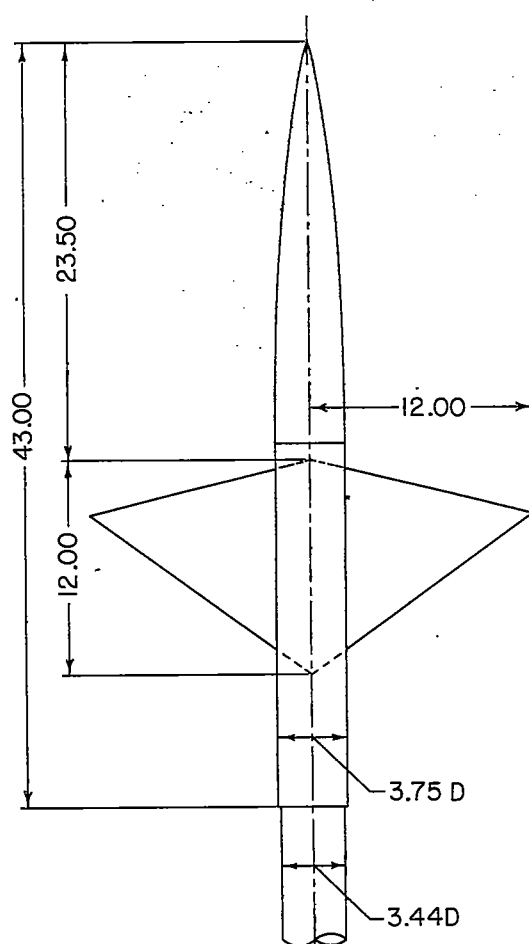
Cylindrical wing-body combination
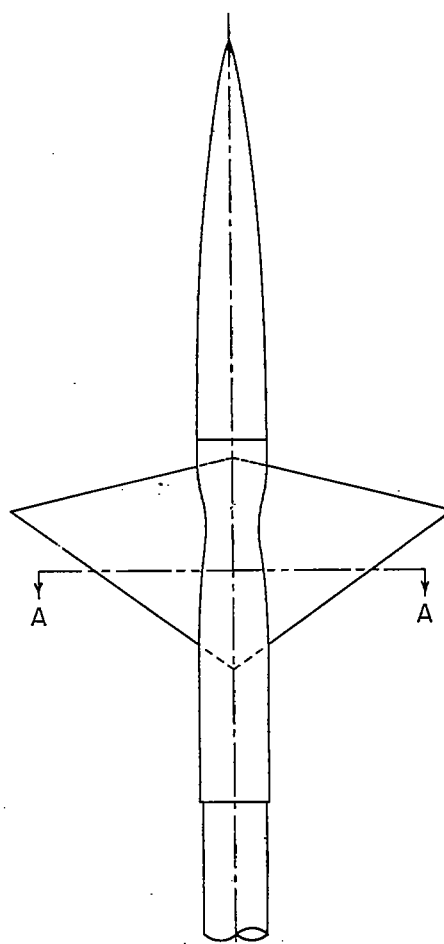
Indented wing-body combination

Wing Details

Airfoil section
 (parallel to plane of symmetry) symmetrical circular arc
Airfoil-section maximum thickness   4 percent
Location of maximum thickness   40 percent chord
Area, sq ft   1
Aspect ratio   4
Taper ratio   0
Incidence, deg   0
Dihedral, deg   0
Geometric twist, deg   0
Sweep of quarter-chord line, deg   0
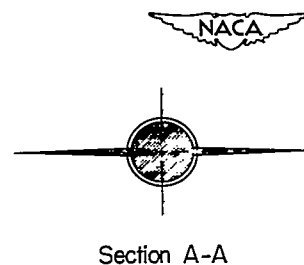
Section A-A

Figure 1.- Plan views and dimensional details of the wing-body combinations
investigated. All dimensions are in inches.
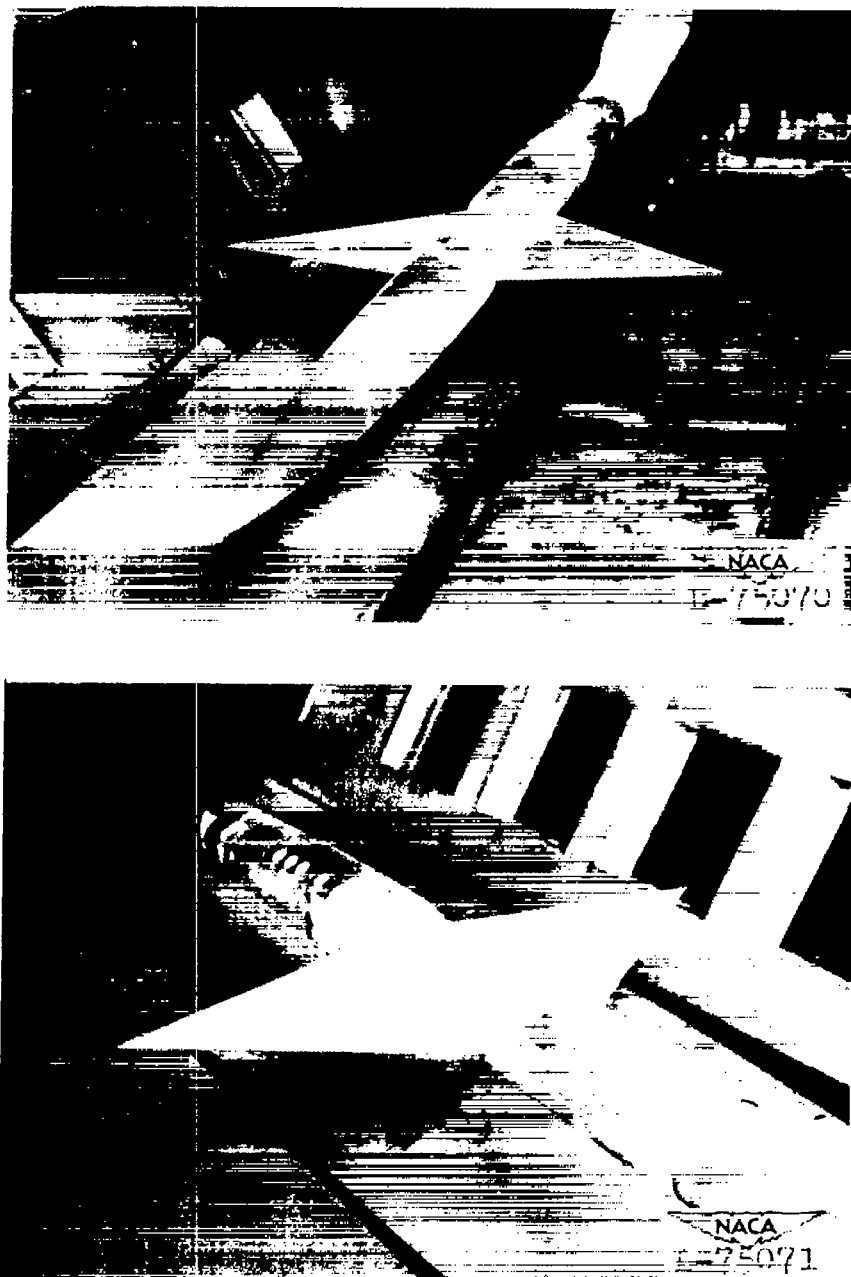
Figure 2.- Front and rear three-quarter views of the indented wing-body combination installed in the Langley 8-foot transonic tunnel.
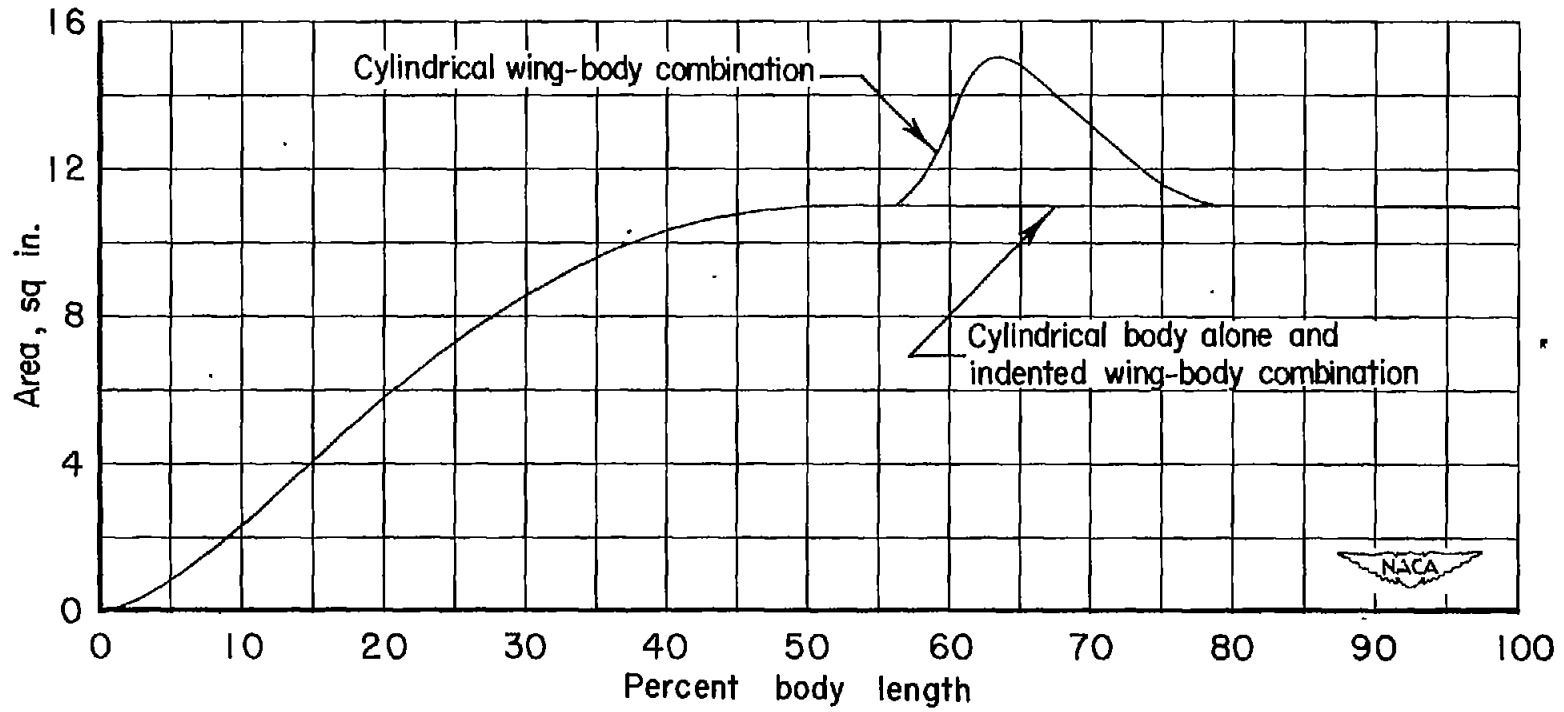
Figure 3.- Axial variations of the cross-sectional areas normal to the axis of symmetry for the models investigated.
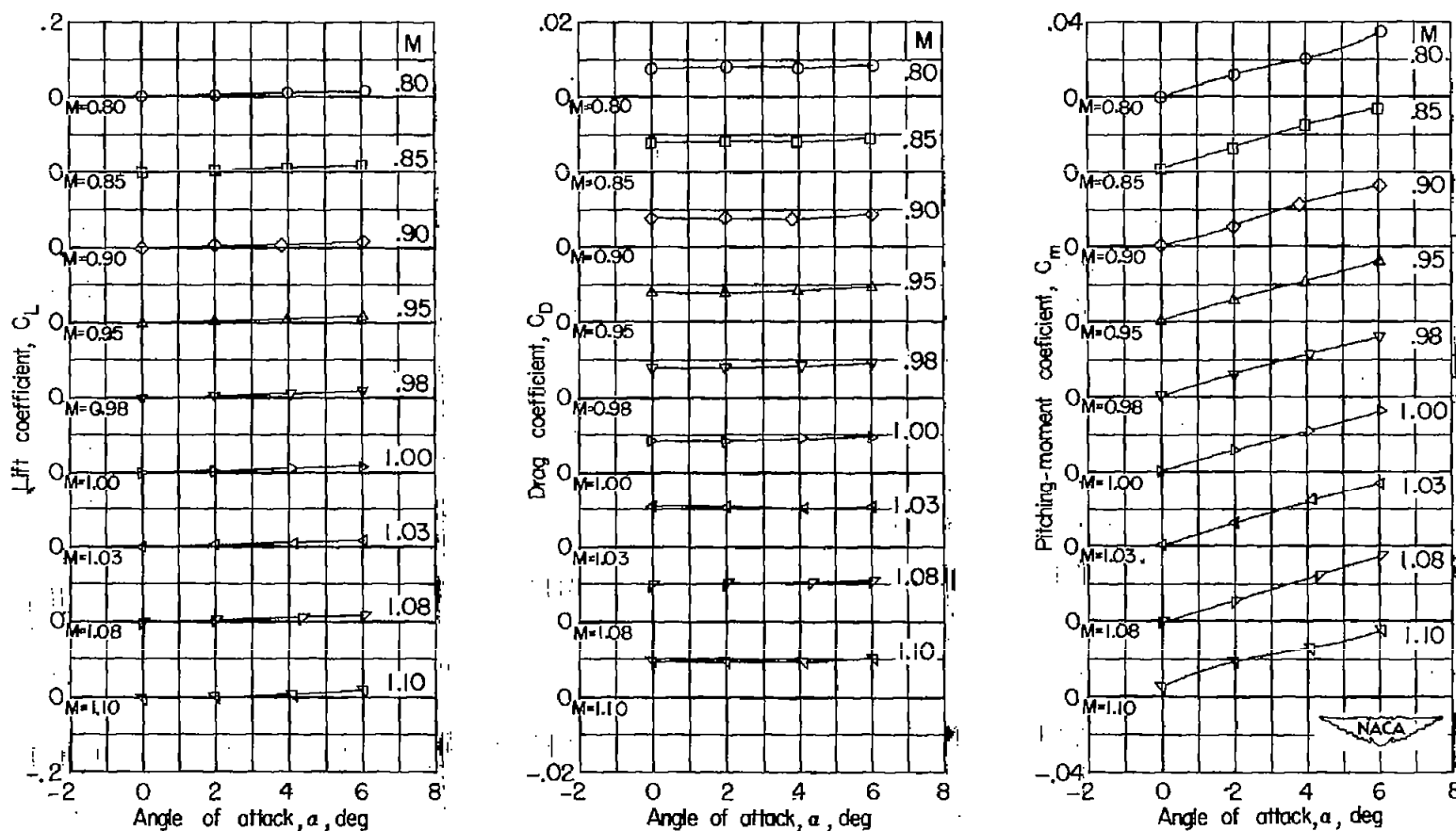
Figure 4.- Basic aerodynamic characteristics for the cylindrical body
alone at several Mach numbers.
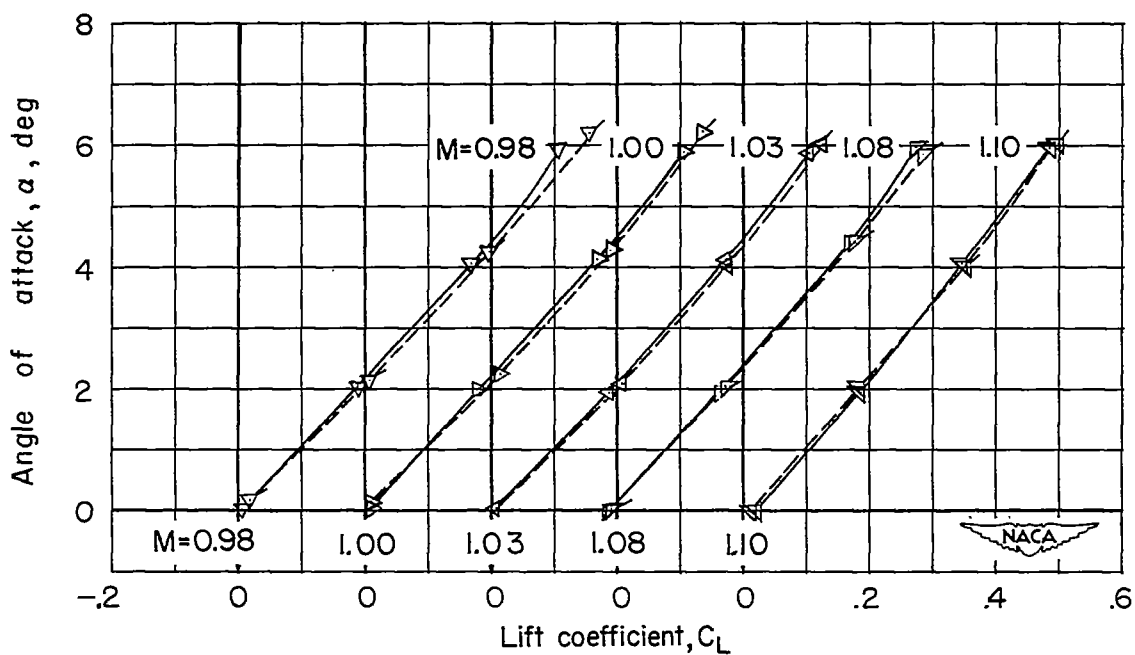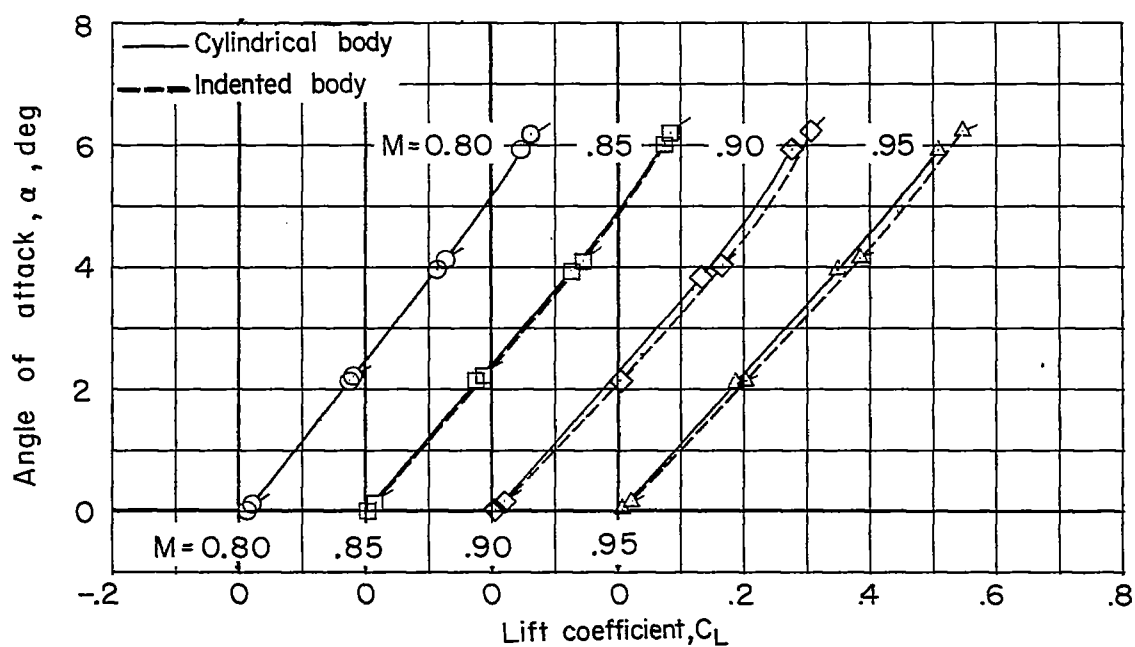
(a) α against C_L.

Figure 5.- Basic aerodynamic characteristics for the cylindrical and
indented wing-body combinations at several Mach numbers.
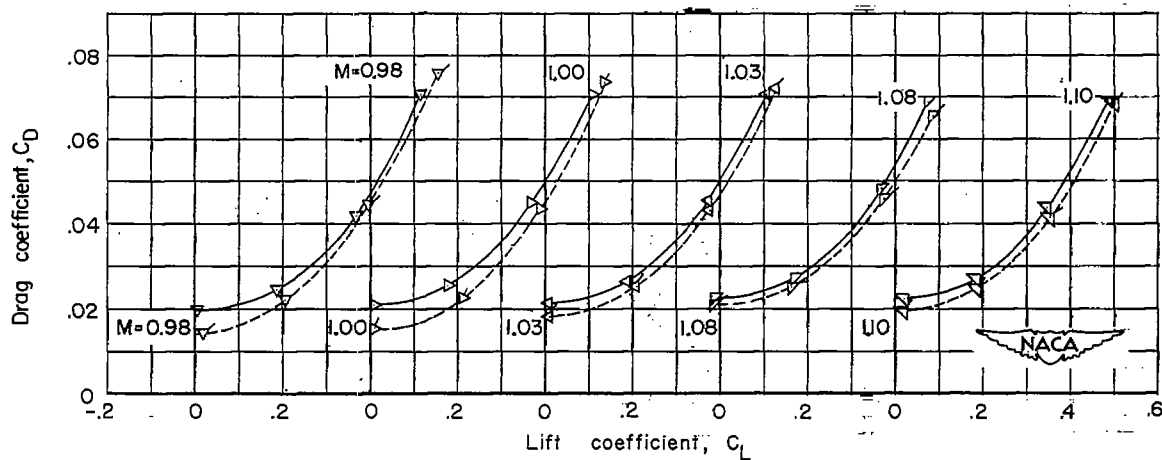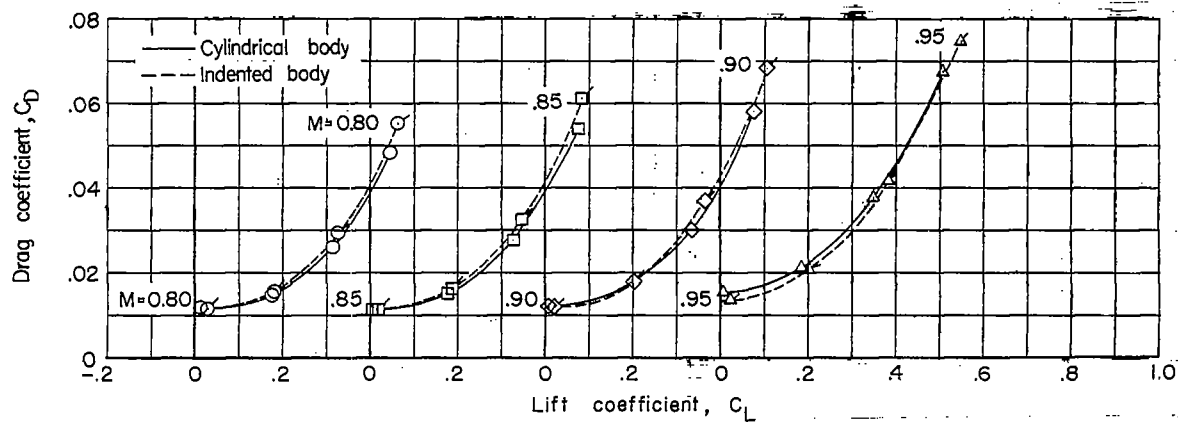
(b) C_D against C_L.

Figure 5.- Continued.
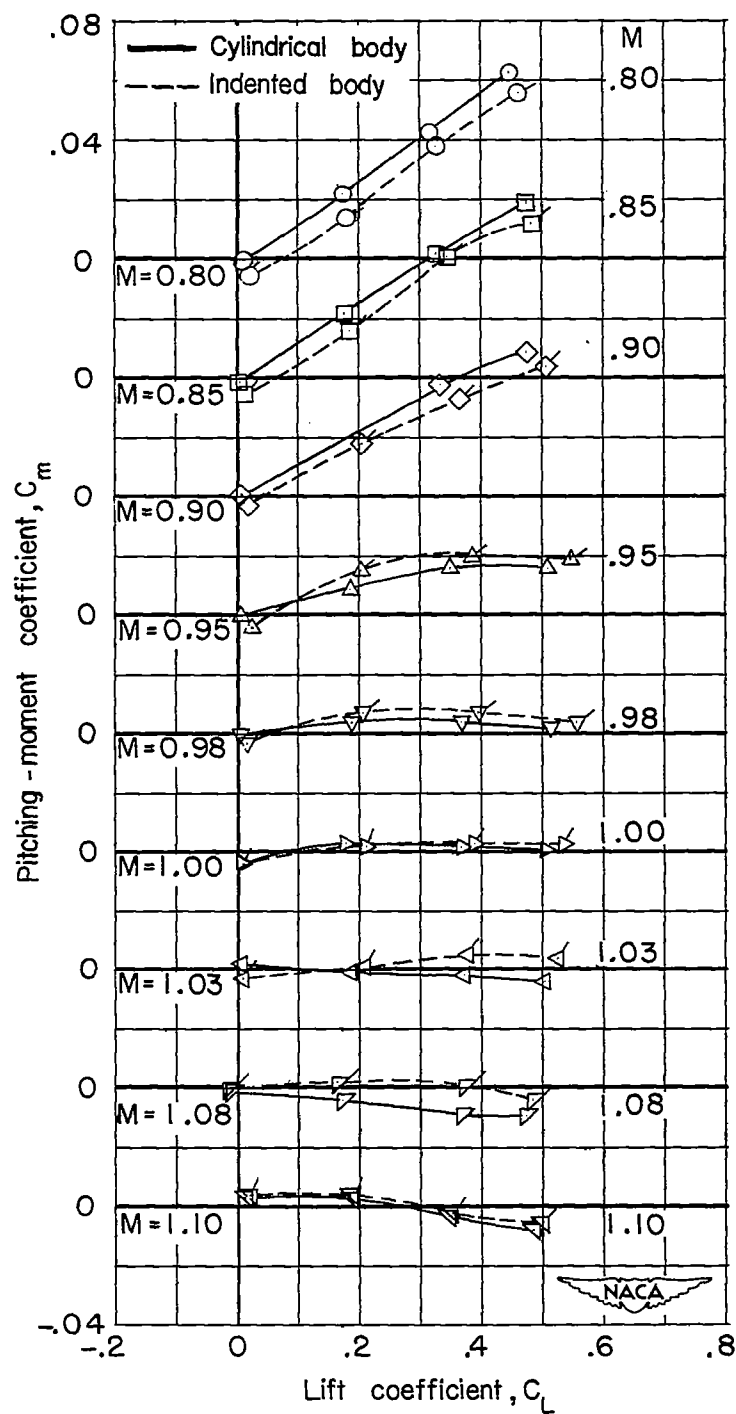
(c) C_m against C_L.

Figure 5.- Concluded.
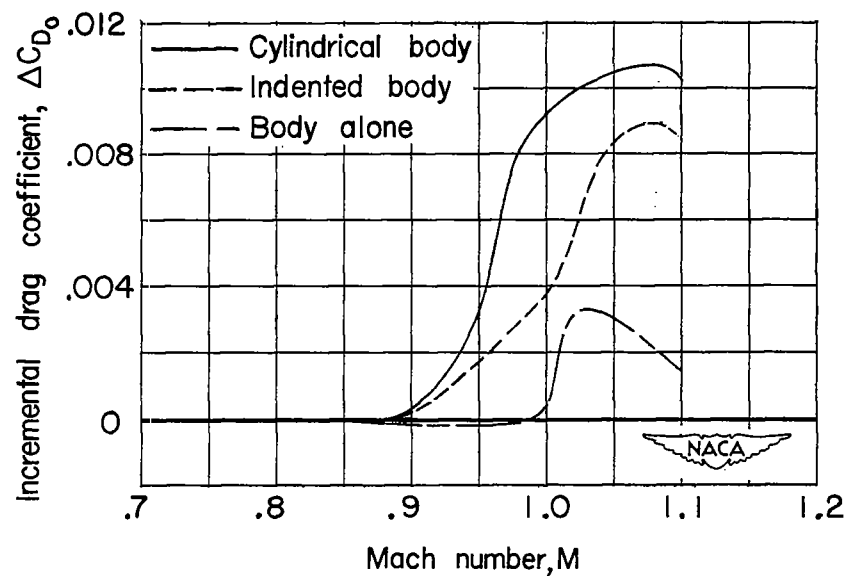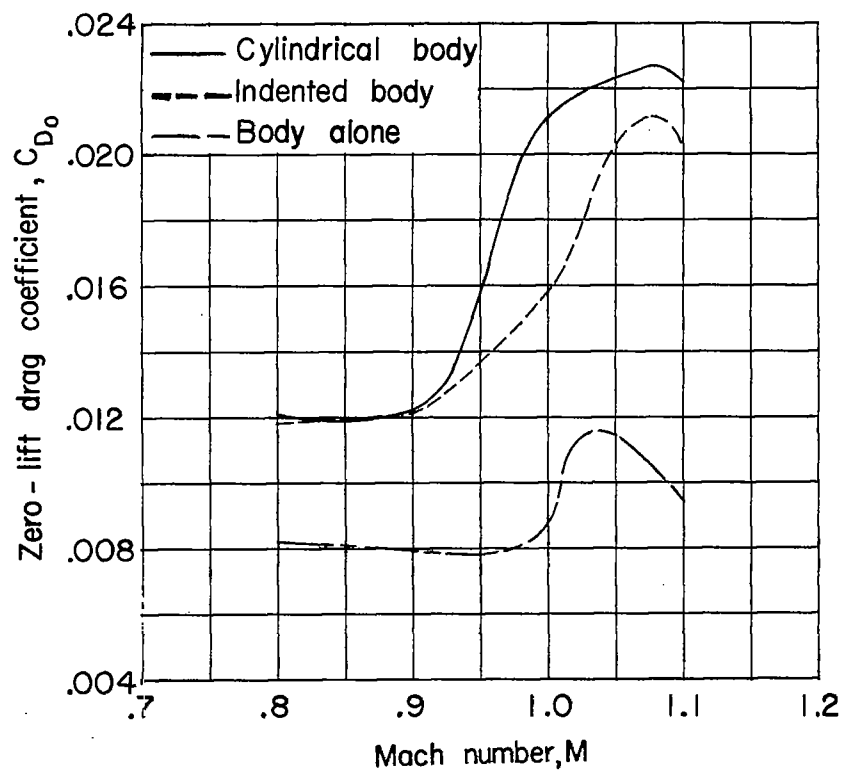
Figure 6.- Drag characteristics at zero lift for the cylindrical and indented wing-body combinations and for the cylindrical body alone. (Data obtained from ref. 1.)
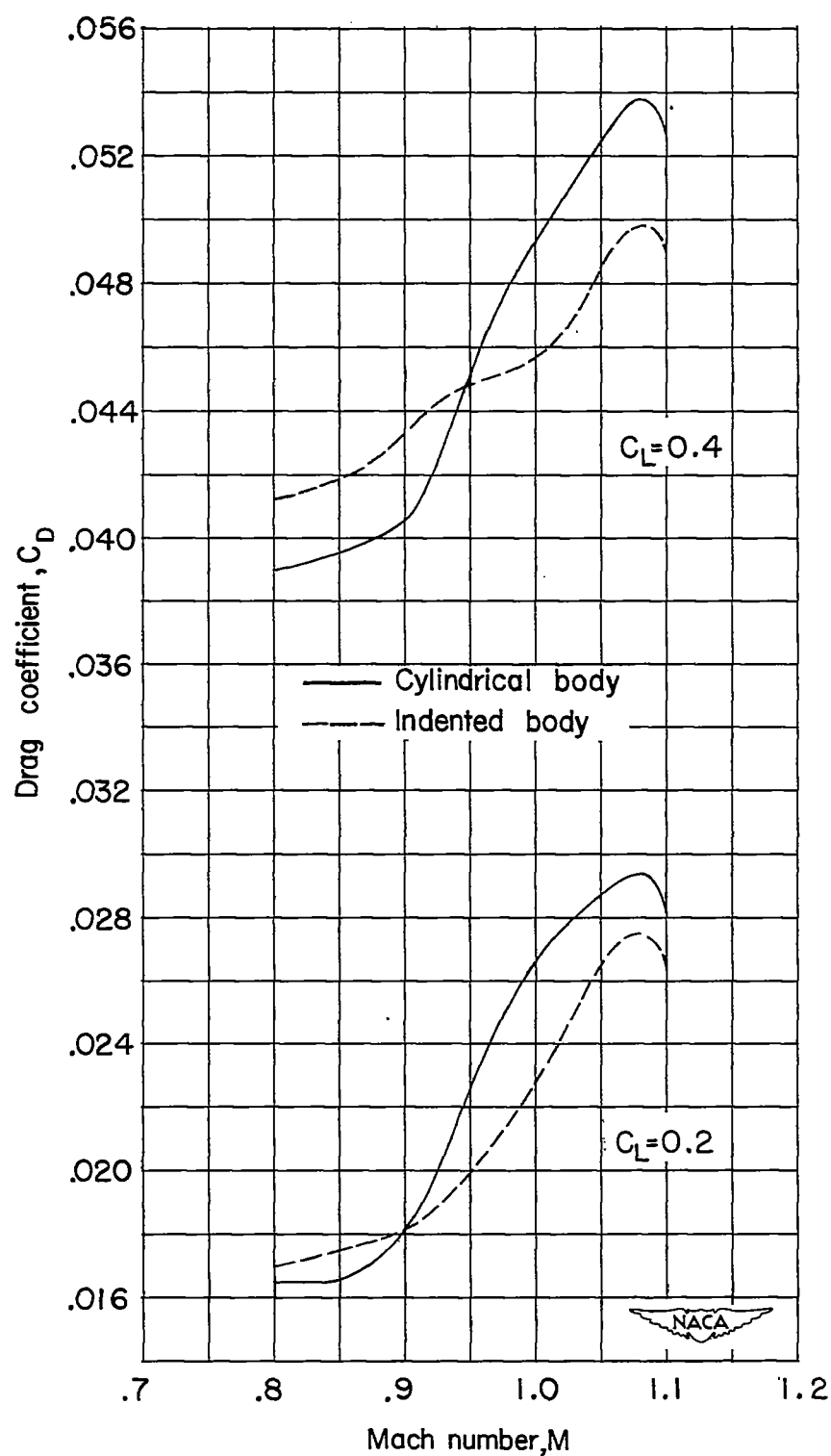
Figure 7.- Drag characteristics at lift coefficients of 0.2 and 0.4 for the wing-body combinations investigated.
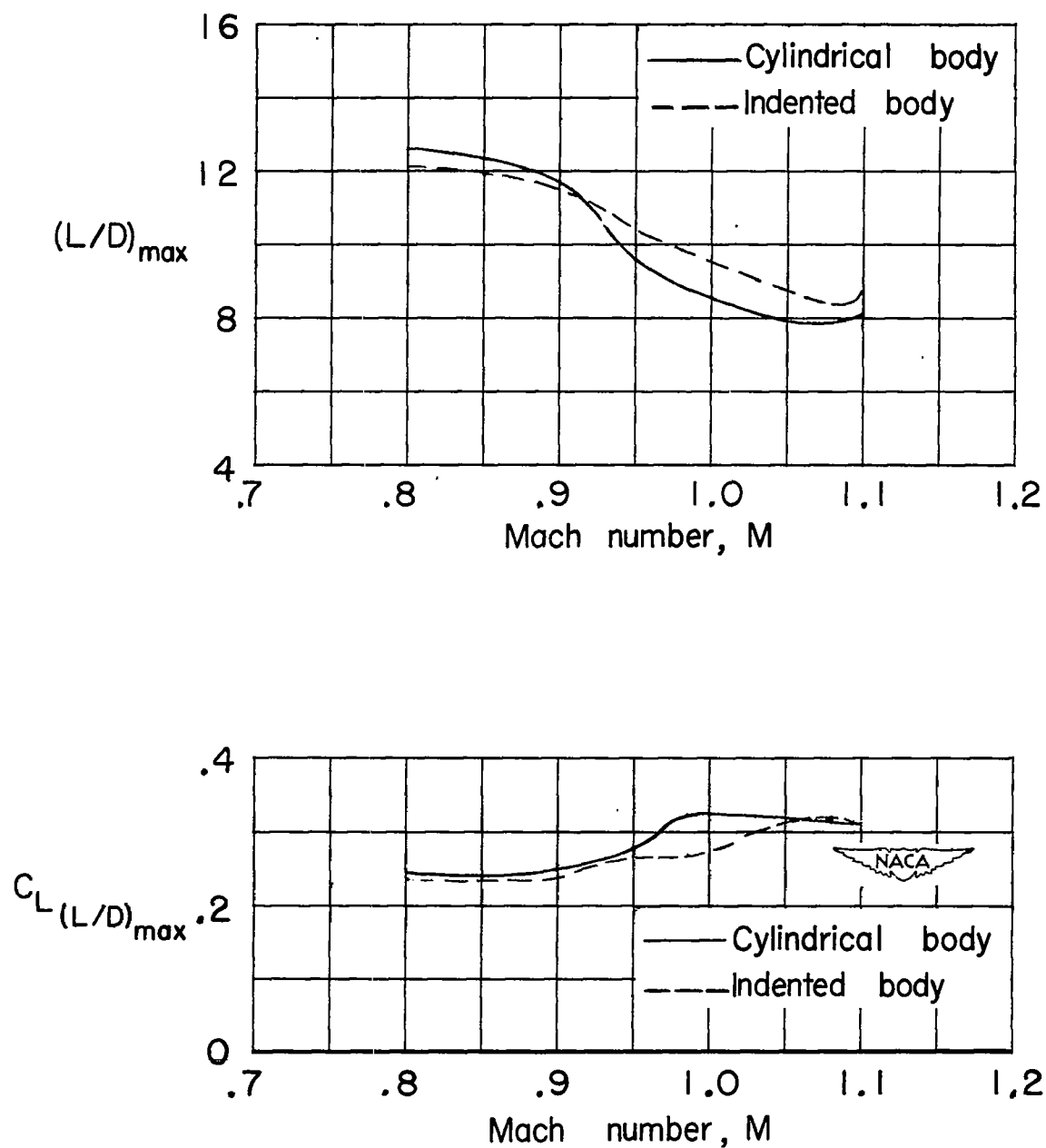
Figure 8.- Comparison of the maximum lift-drag ratio and lift coefficients for maximum lift-drag ratio for the wing-body combinations investigated.
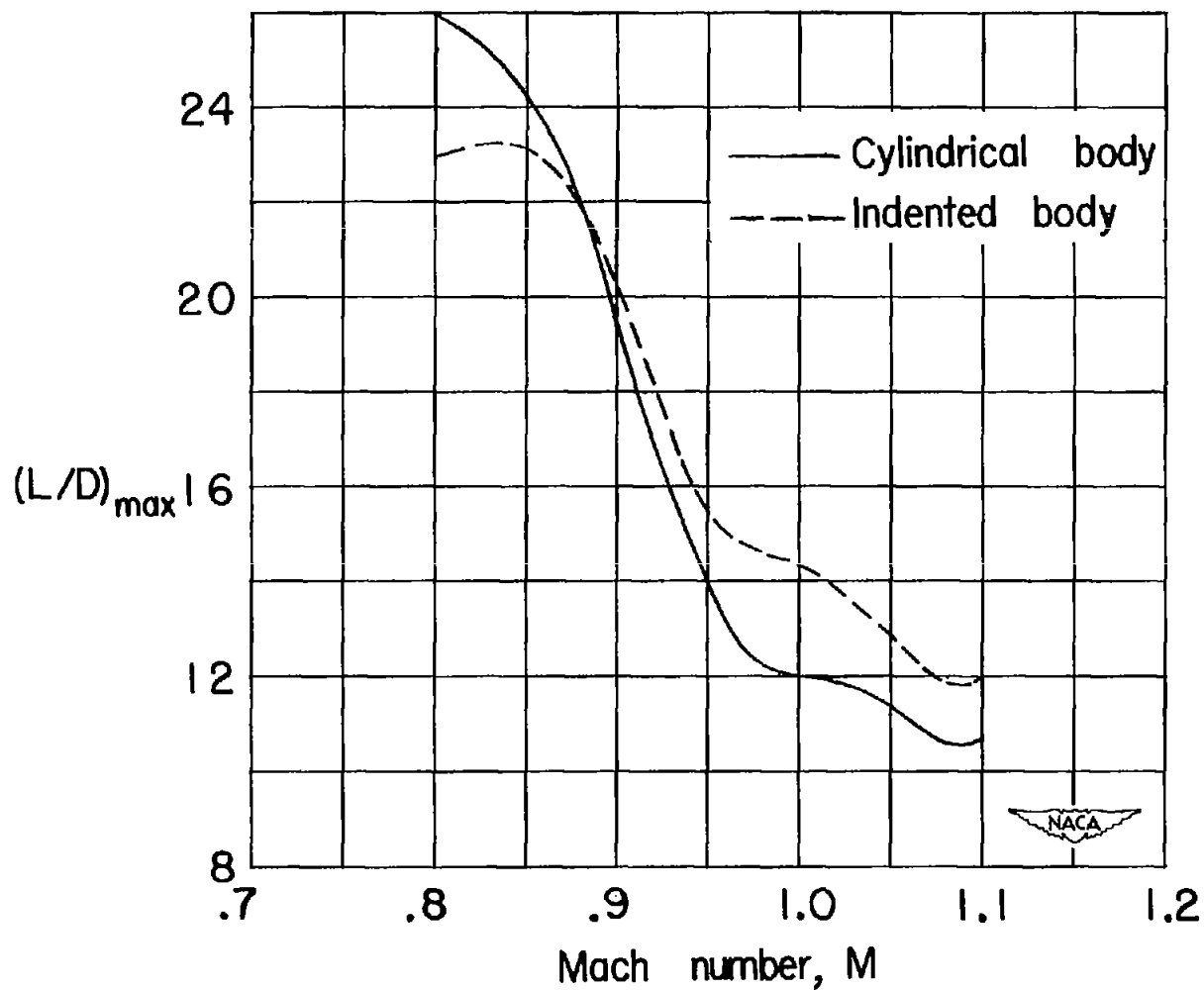
Figure 9.- Comparison of the maximum wing-plus-interference lift-drag ratio for the wing-body combinations investigated.
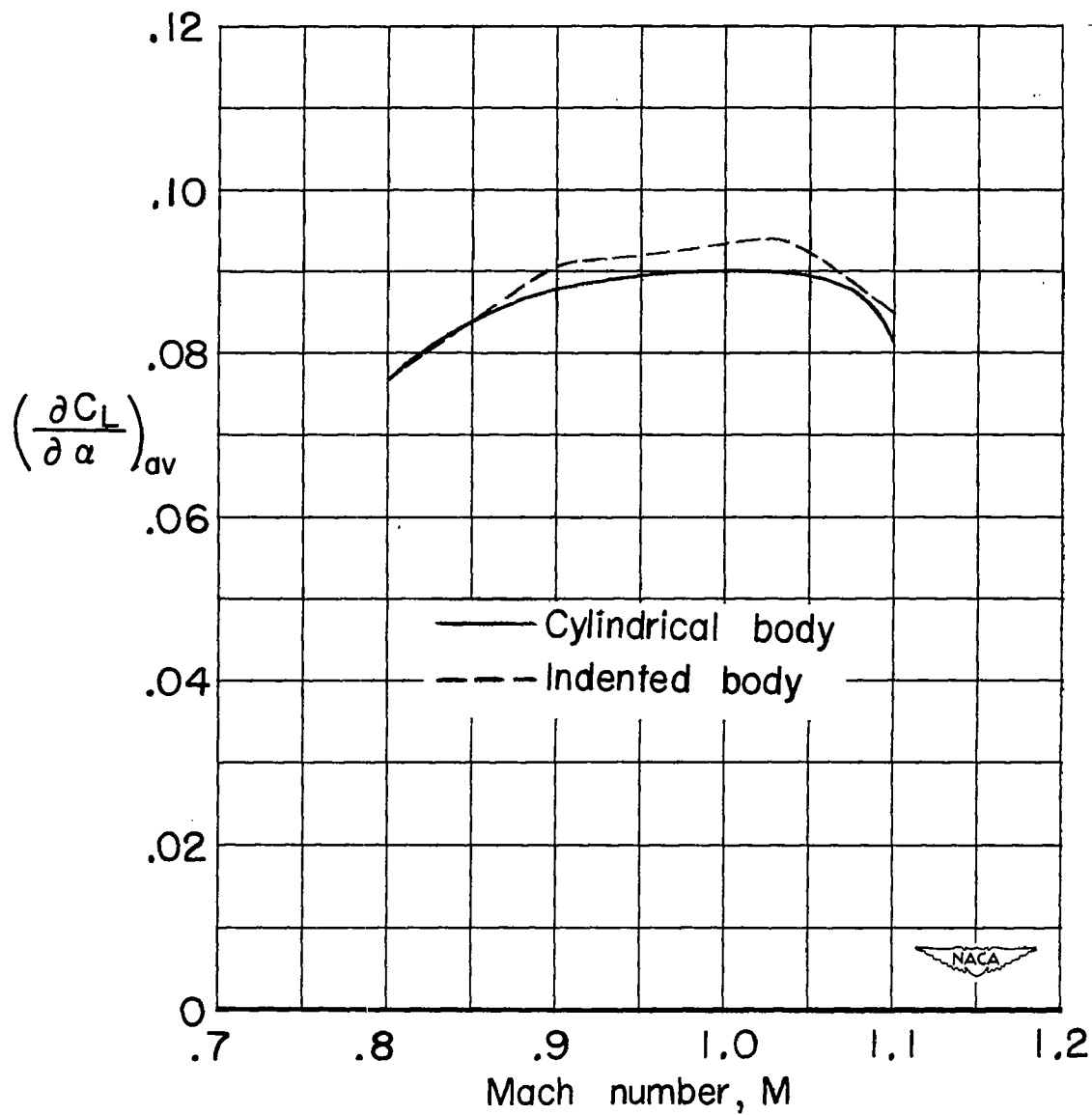
Figure 10.- Average lift-curve slope comparisons for the wing-body combinations.
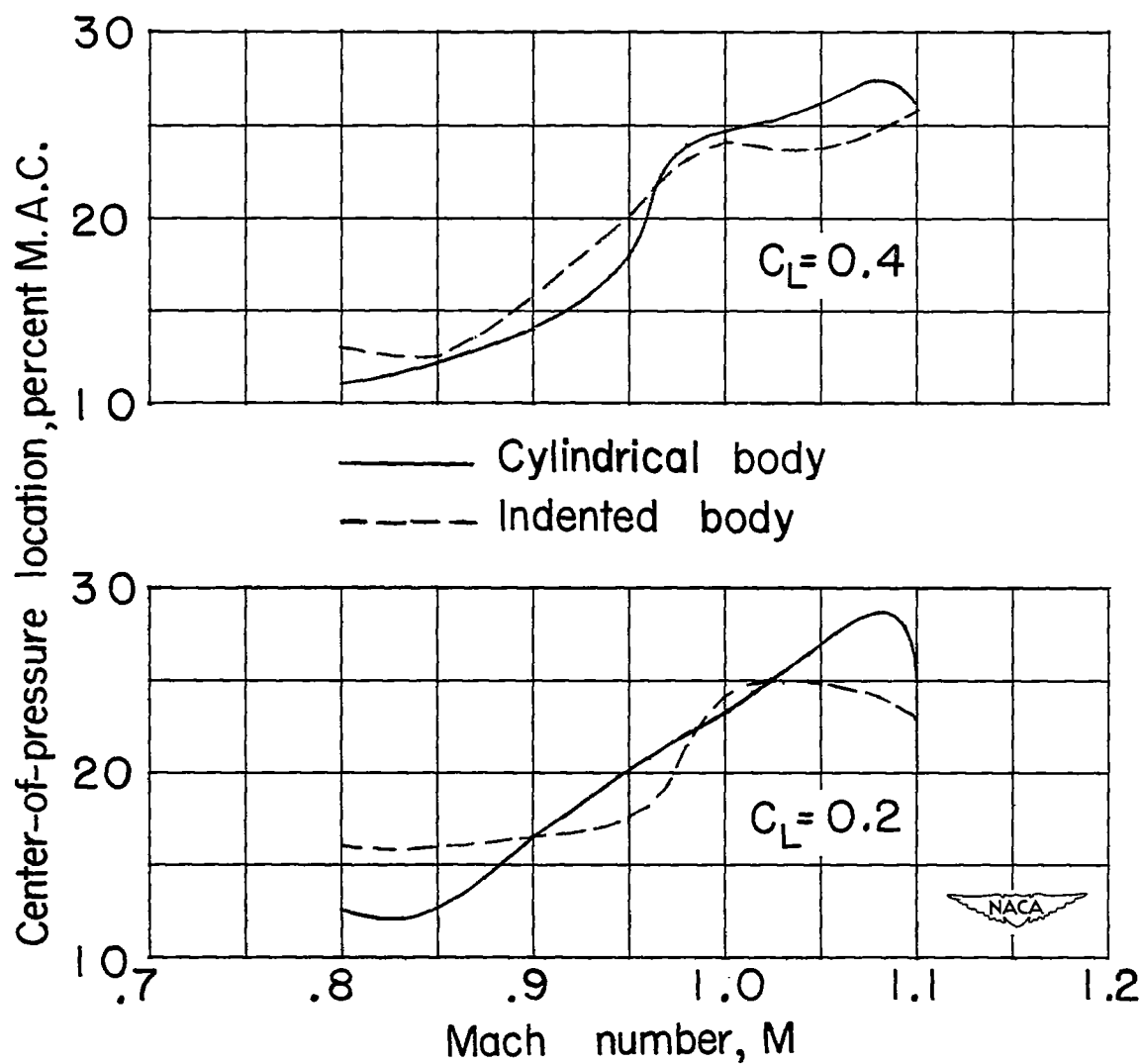
Figure 11.- Variations of the location of the center of pressure at
lift coefficients of 0.2 and 0.4 for the wing-body combinations.

Tunnel wall

Model

Schlieren field

Side view

Tunnel configuration for side view
schlieren surveys

Plan view

Locations of M_w survey stations

Tunnel configuration for plan view
schlieren surveys

M_w

Stream Mach number

M_w

Stream Mach number
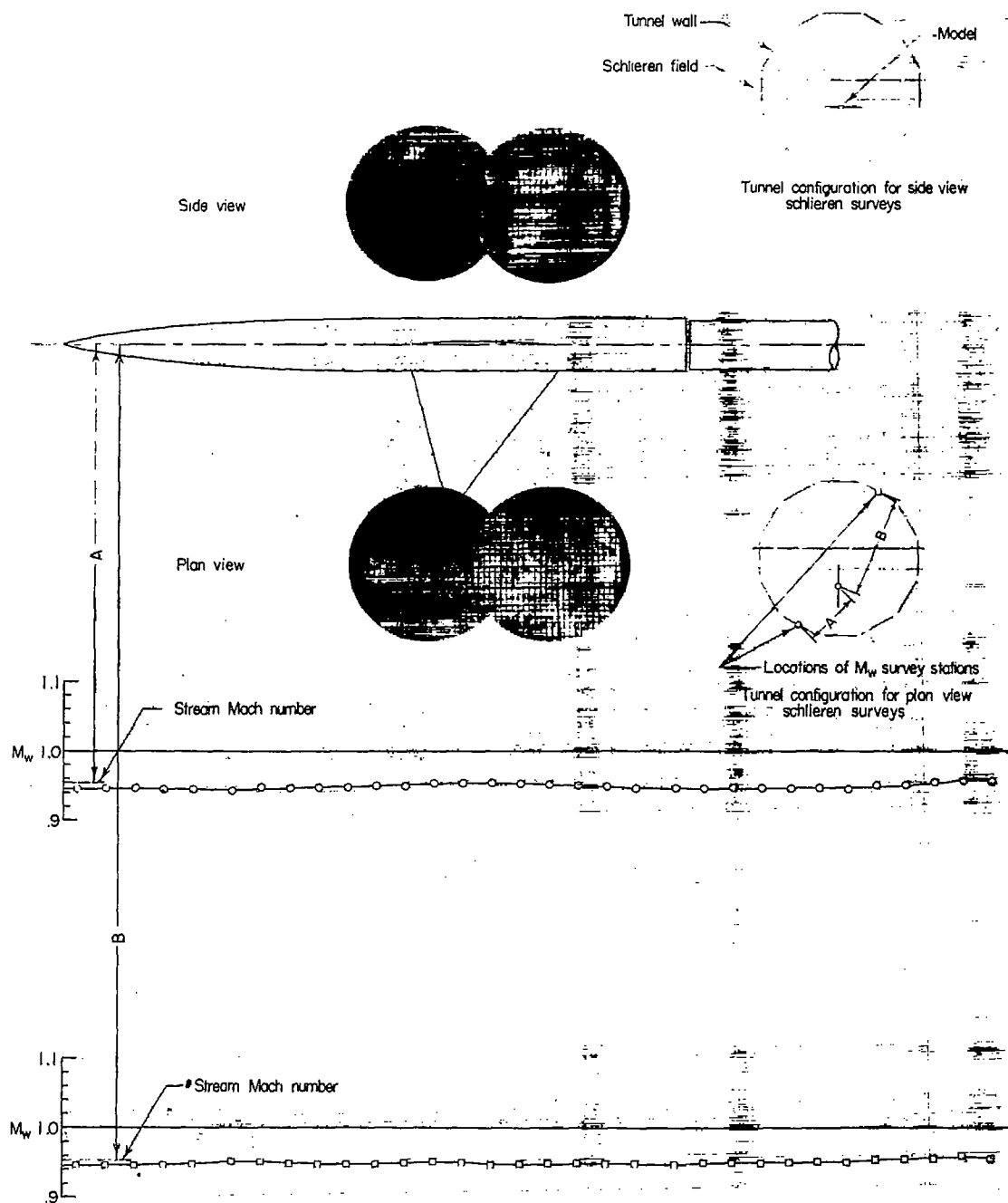
(a) Cylindrical body, $M_0 = 0.95$.

L-77876

Figure 12.- Comparison of the shock-wave phenomena for the wing and
cylindrical body with those for the wing and indented body at an
angle of attack of 0°.

Side view

Plan view

M_w 1.1

M_w 1.0

.9

M_w 1.1

M_w 1.0

.9
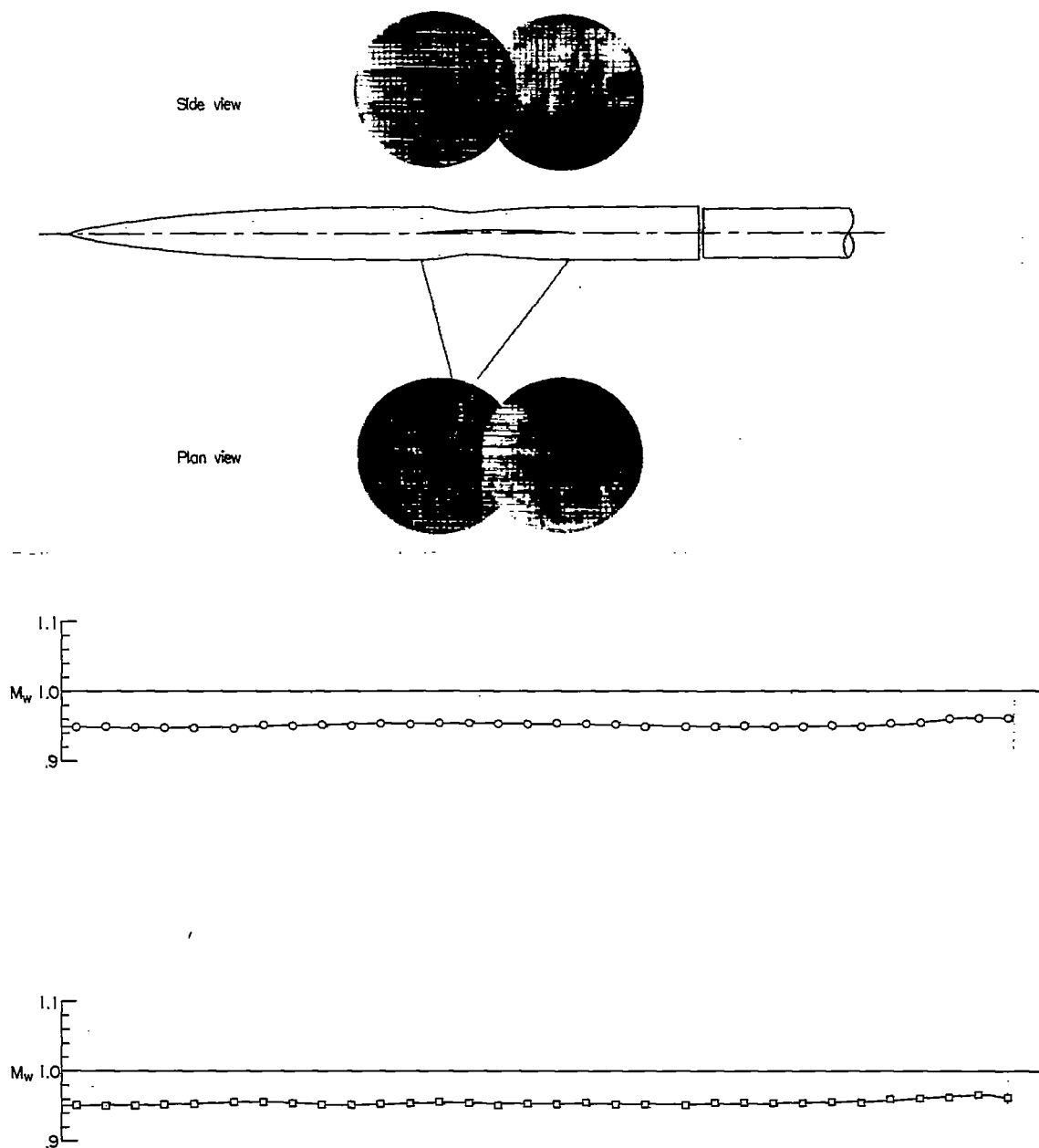
(b) Indented body, $M_O = 0.95$.

Figure 12.- Continued.
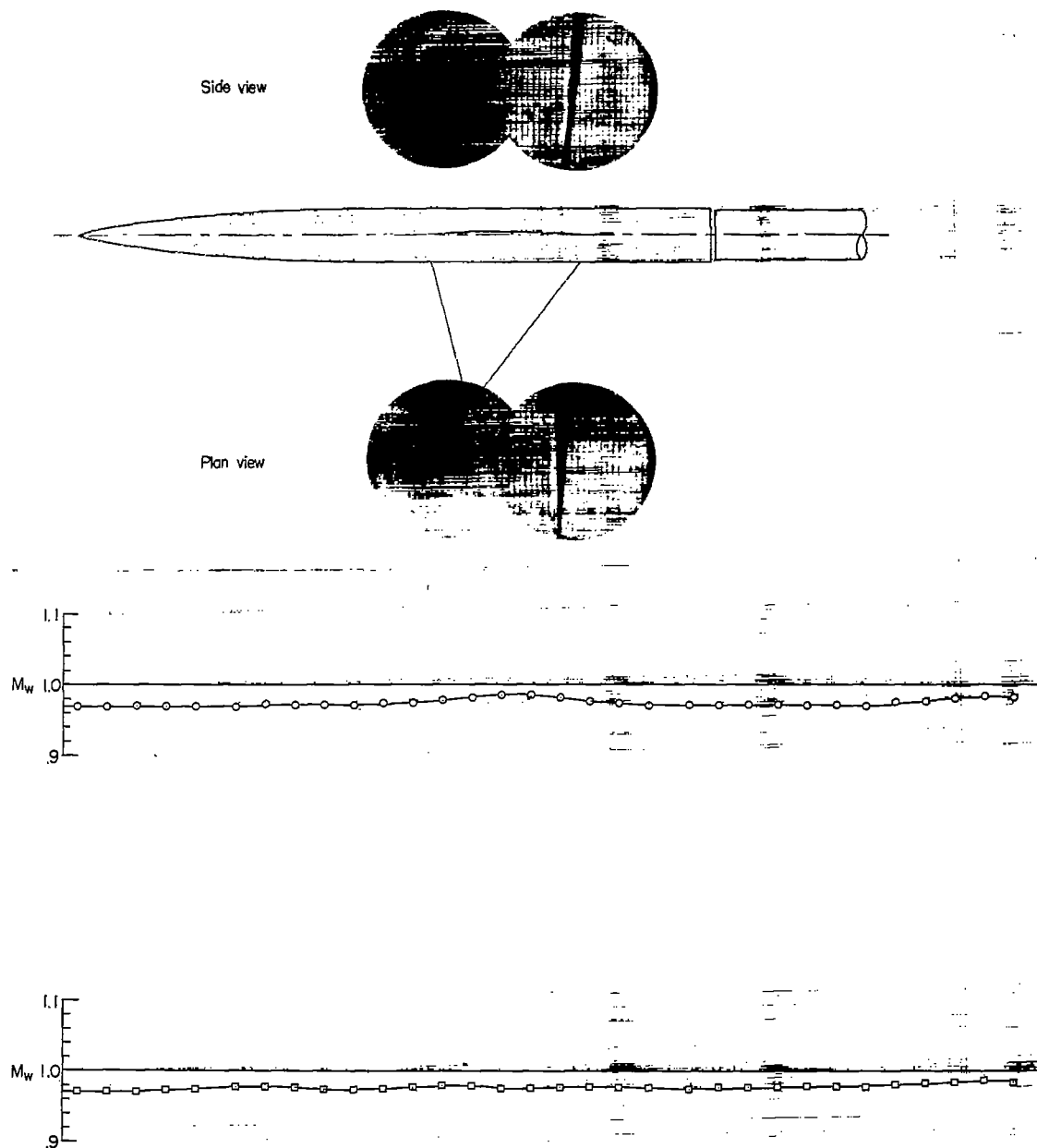
L-77877

(c) Cylindrical body, $M_O = 0.98$.

Figure 12.- Continued.
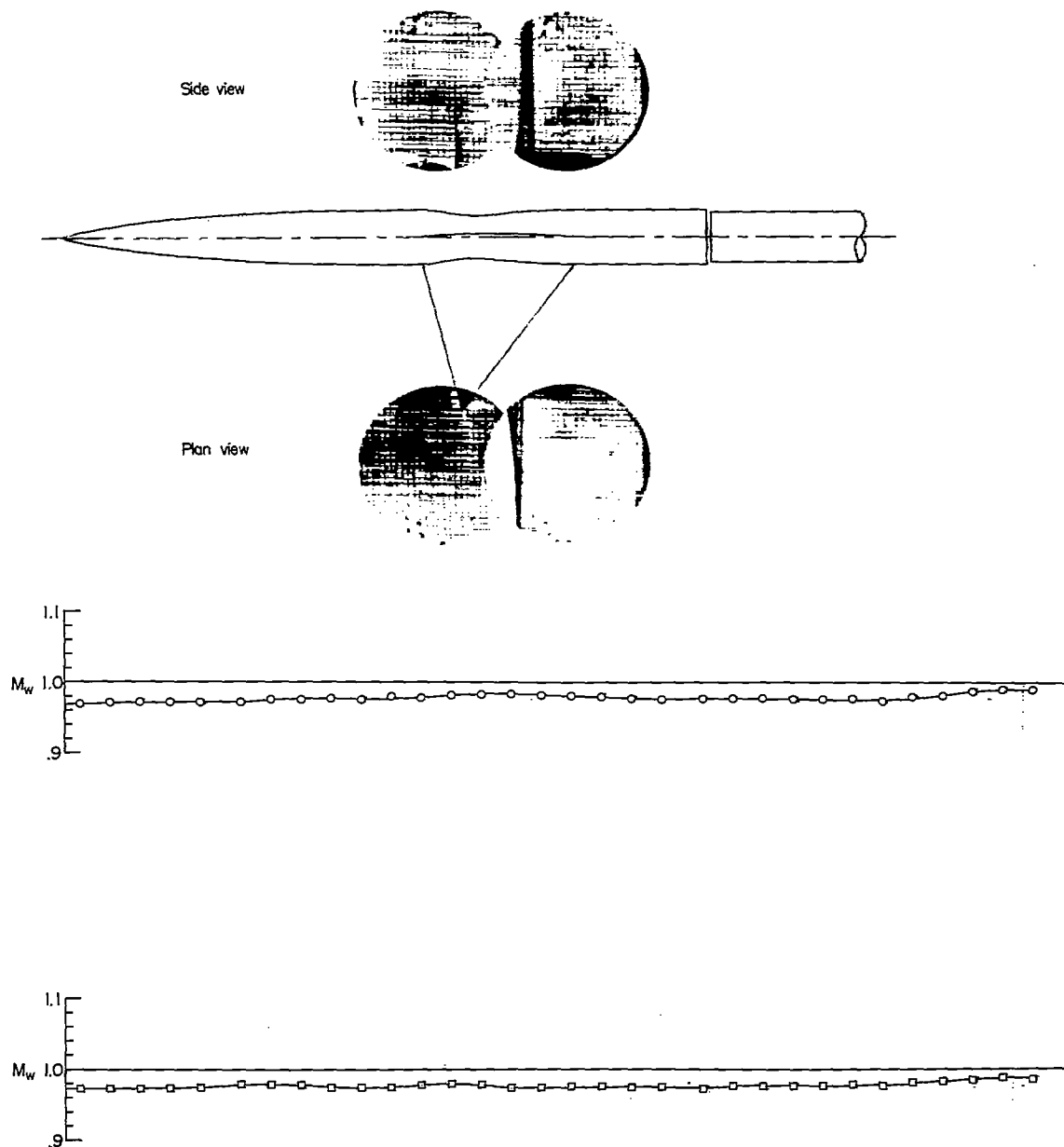
L-77878

Side view

Plan view

(d) Indented body, $M_O = 0.98.$

Figure 12.- Continued.

L-77879

Side view

Plan view

M_w 1.0

M_w 1.0
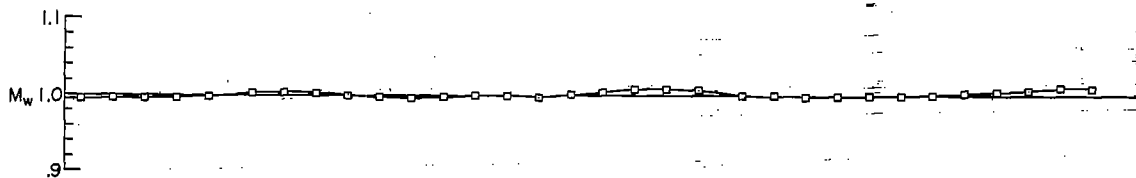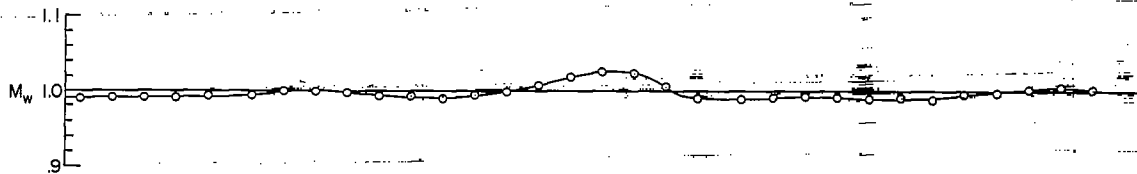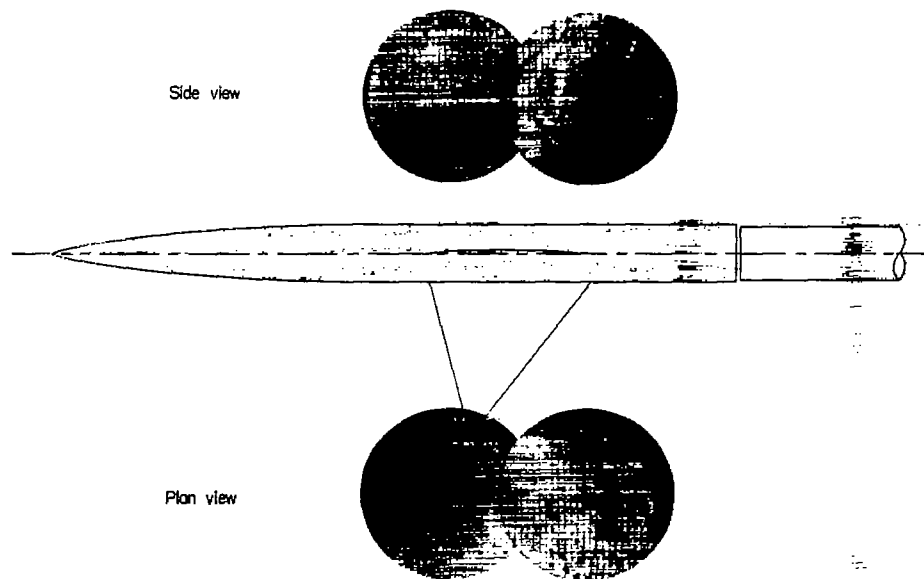
(e) Cylindrical body, M_O = 1.00.

Figure 12.- Continued.
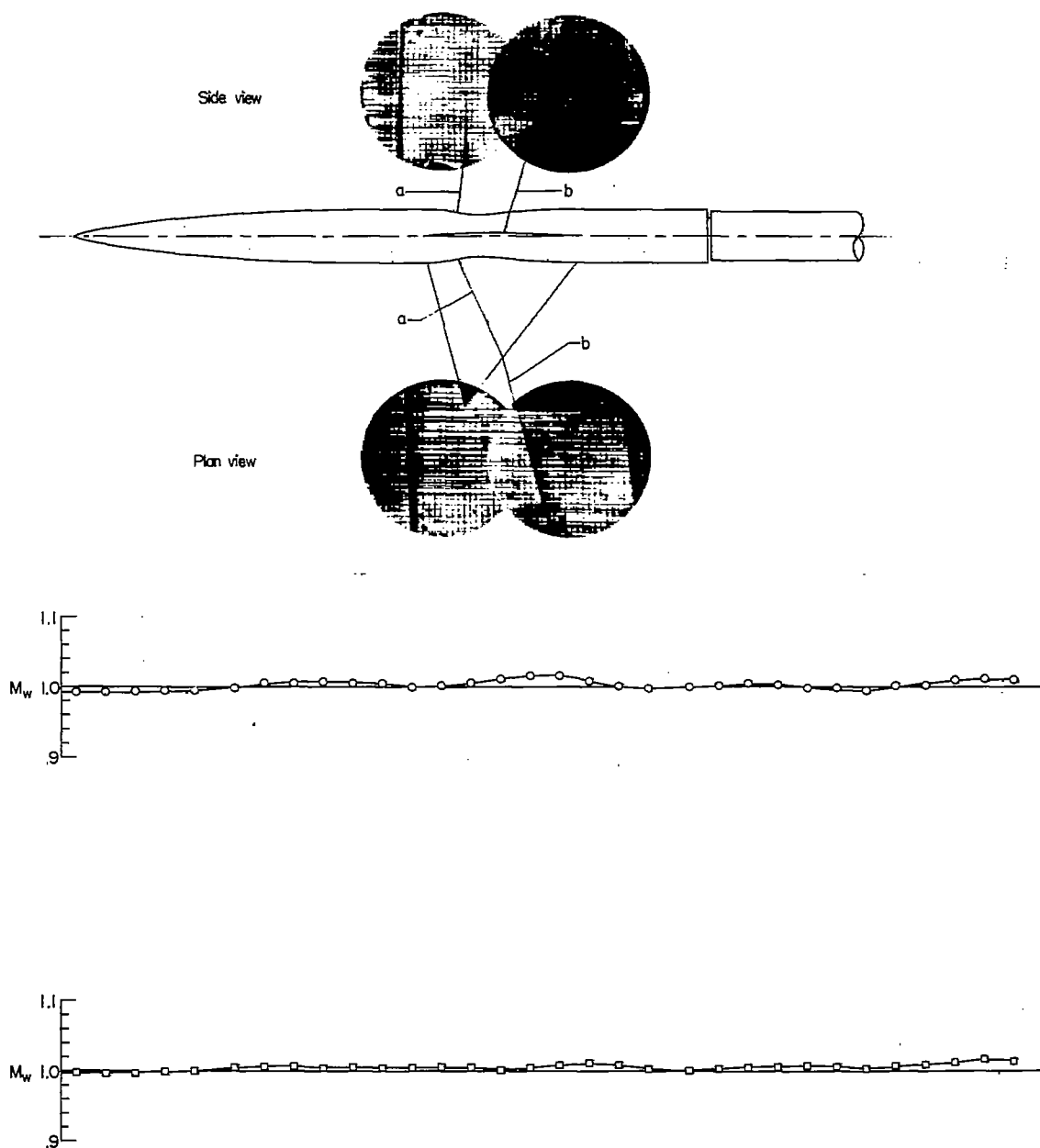
L-77880
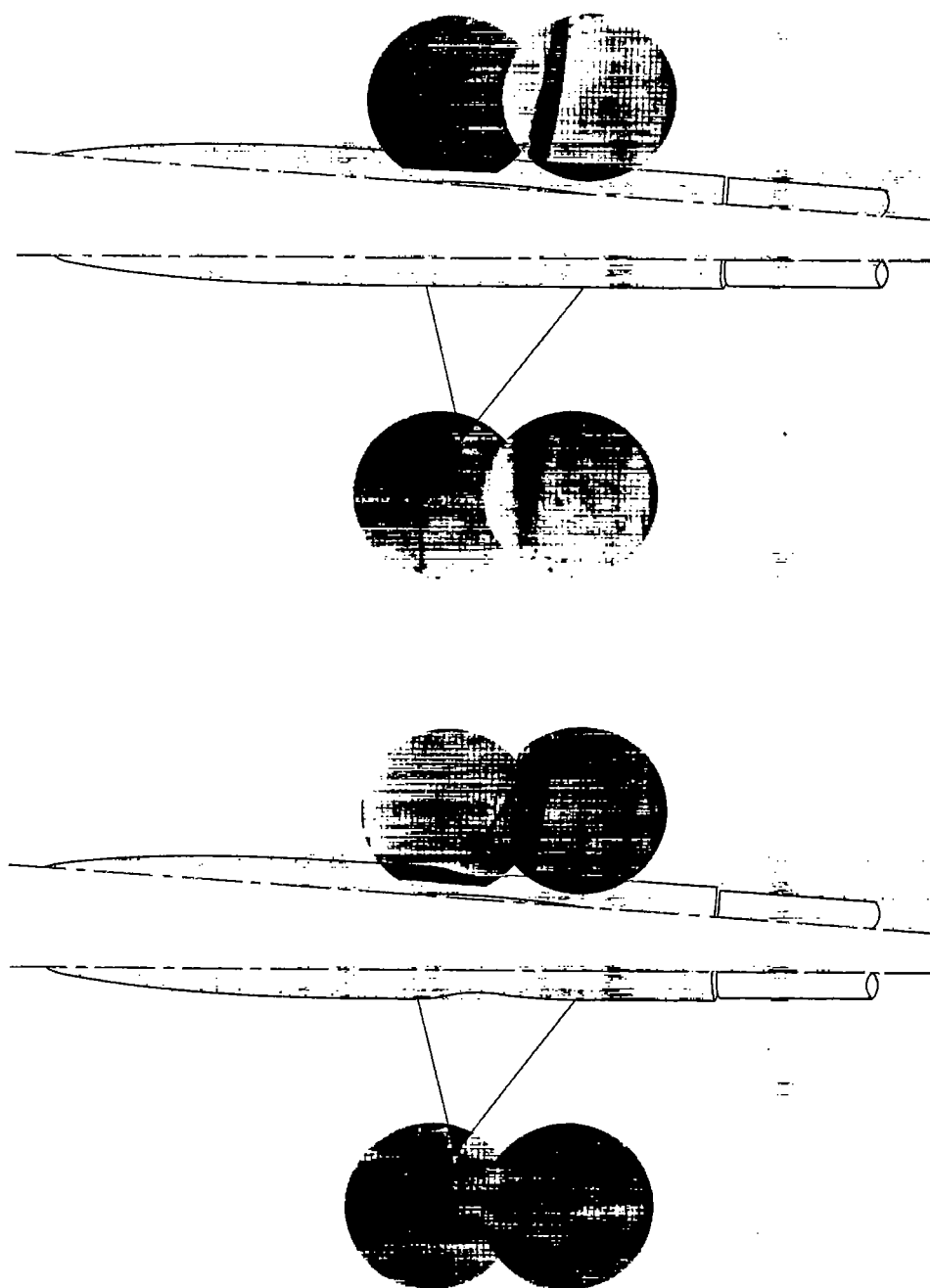
(f) Indented body, $M_O = 1.00$.

Figure 12.- Continued.
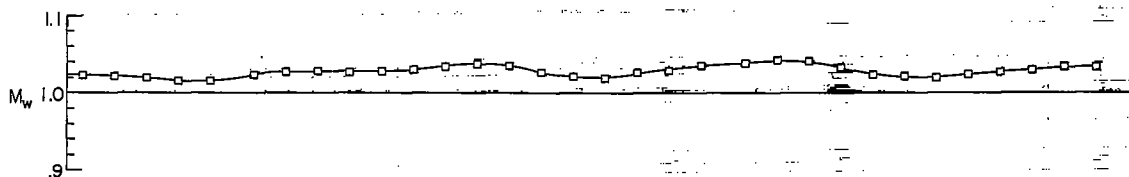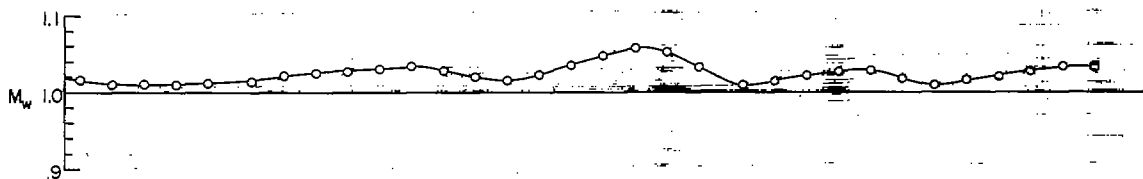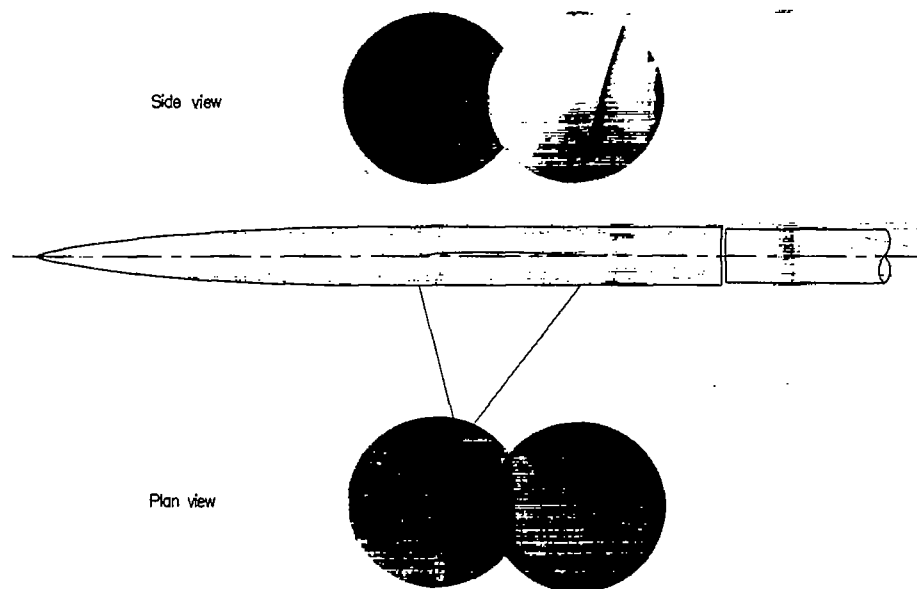
L-77881

(g) Cylindrical body, $M_O = 1.03$.

Figure 12.- Continued.
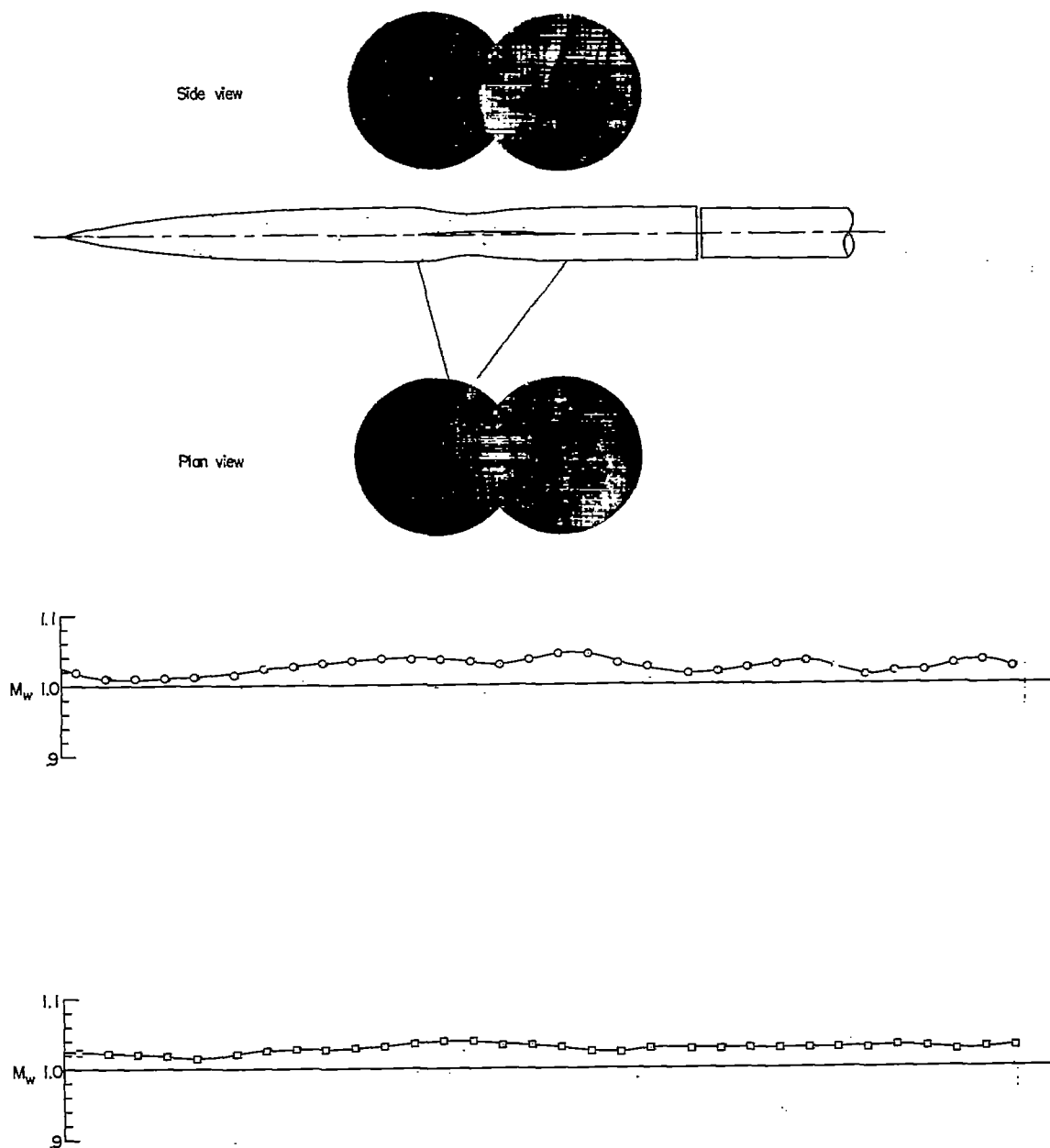
L-77882

(h) Indented body, $M_O = 1.03$.

Figure 12.- Continued.
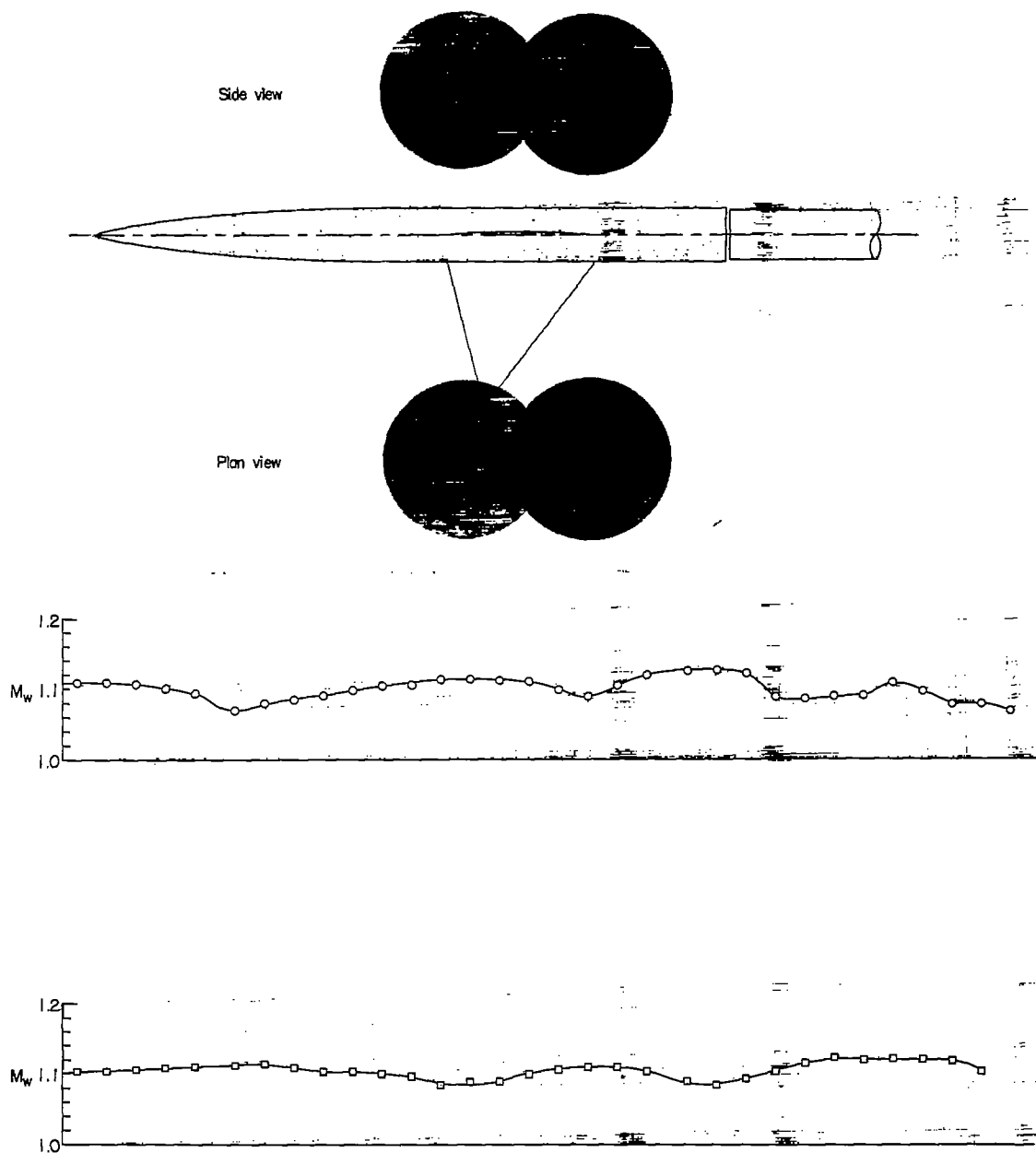
L-77883

(1.) Cylindrical body, $M_O = 1.10$.

Figure 12.- Continued.
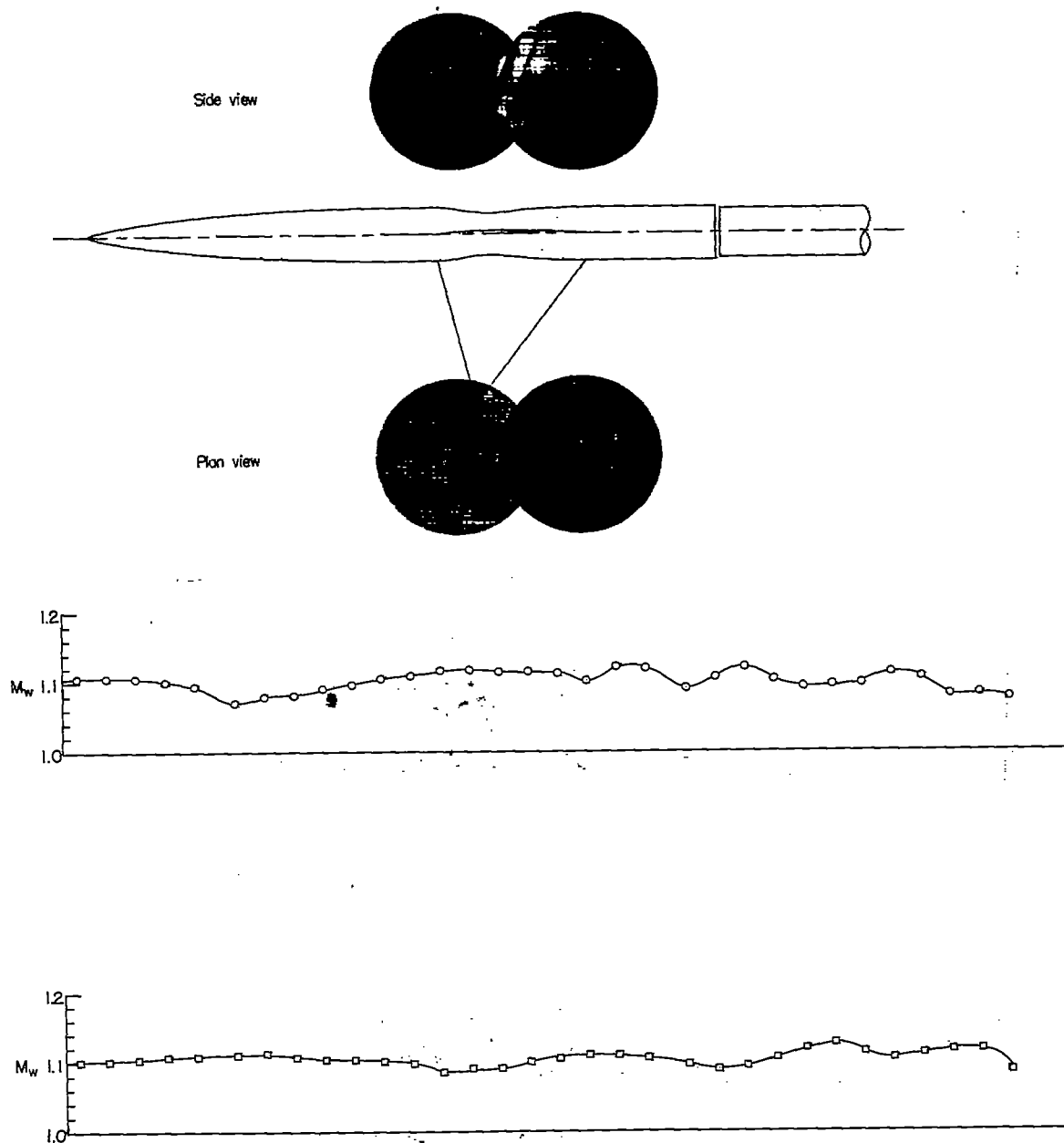
L-77884

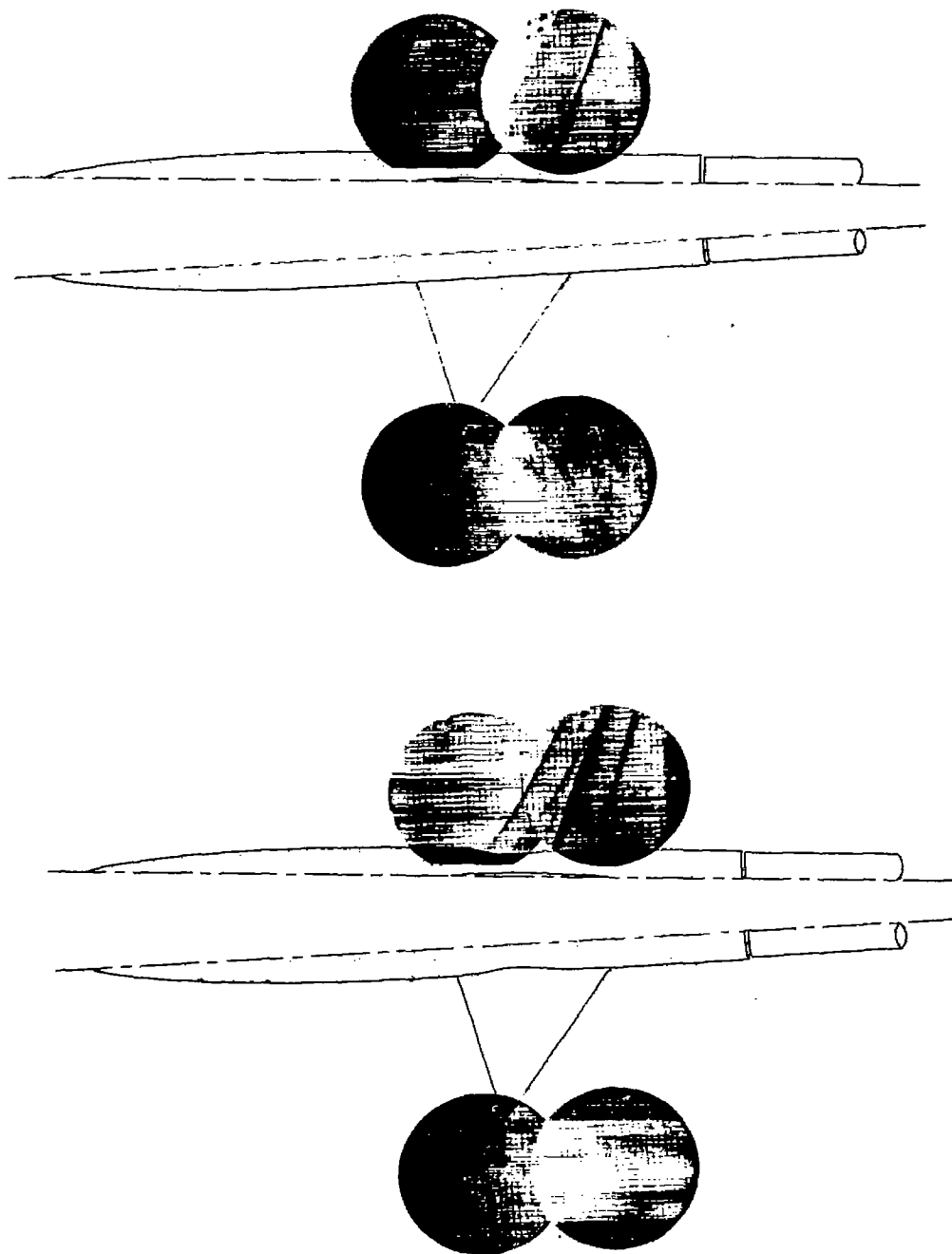(j) Indented body, $M_O = 1.10$.

Figure 12.- Concluded.

L-77885

(a) $M_0 = 0.95$.

L-77886

Figure 13.- Comparison of the shock-wave phenomena for the wing and
   cylindrical body with those for the wing and indented body at an
   angle of attack of 4.0°.

(b) $M_0 = 1.00$.

Figure 13.- Continued.
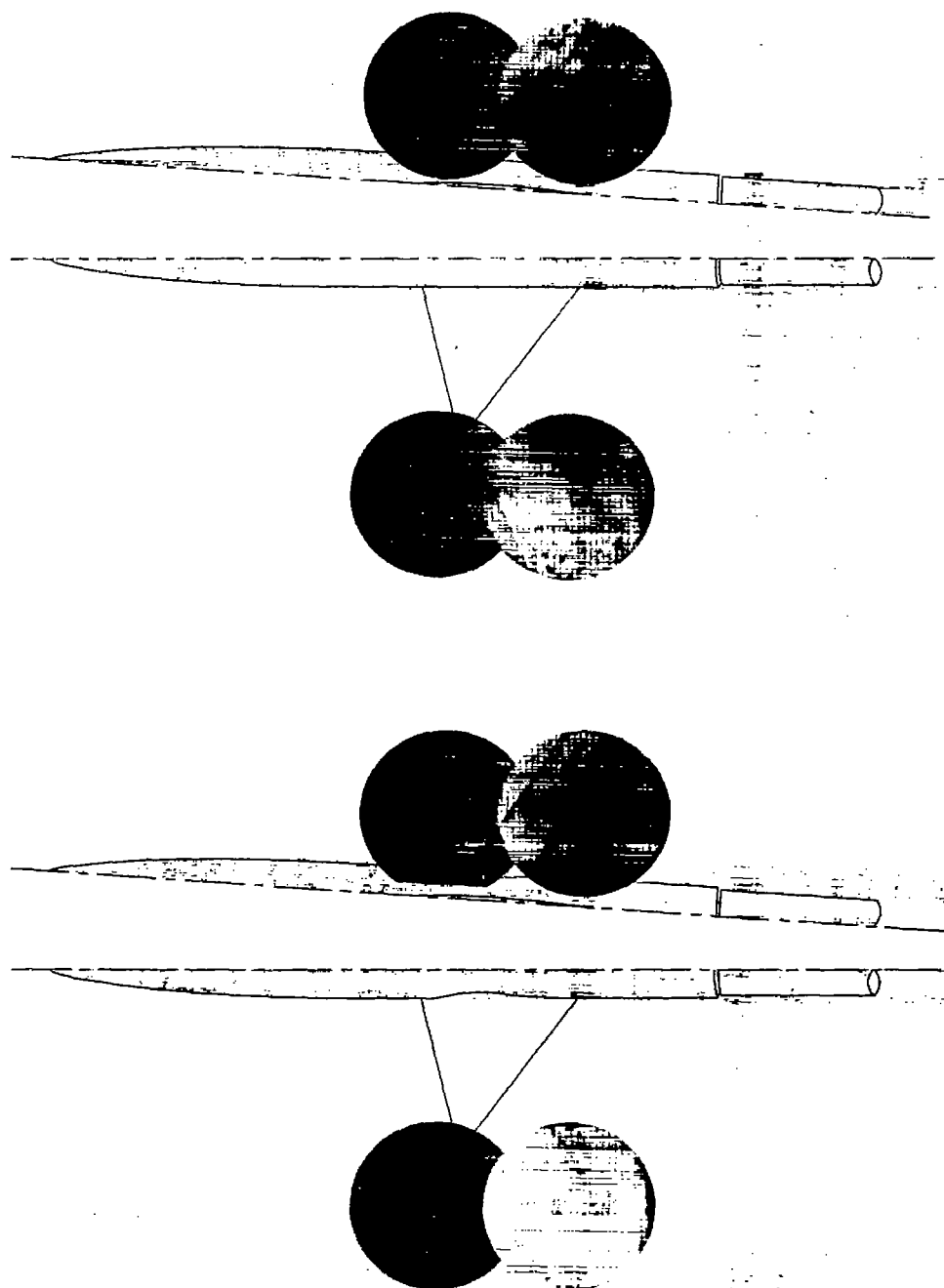
L-77887

(c) $M_O = 1.10$.

Figure 13.- Concluded.   L-77888